PHENOMENOLOGICAL MODELLING OF FLOW BEHAVIOUR OF ARMOUR STEEL MATERIAL AT ELEVATED TEMPERATURES WITH DIFFERENT STRAIN RATES

Thesis is submitted in partial fulfilment of the requirement for the degree of

MASTER OF MECHANICAL ENGINEERING

By:

MD RAKIM

Examination Roll No.: M4MEC22001

Registration No.: 131706 of 2015-16

Under the guidance of:

Prof. SANJIB KUMAR ACHARYYA

Department of Mechanical Engineering

Faculty of Engineering and Technology

Jadavpur University

Kolkata-700032

June, 2022

FACULTY OF ENGINEERING AND TECHNOLOGY

DEPARTMENT OF MECHANICAL ENGINEERING

JADAVPUR UNIVERSITY

KOLKATA -700032

DECLARATION OF ORIGINALITY AND COMPLIANCE OF ACADEMIC ETHICS

I hereby declare that this thesis contains literature survey and original research work by the undersigned candidate, as part of his Master of mechanical engineering (Machine Design) studies.

All information in this document have been obtained and presented accordance with academic rules and ethical conduct.

I also declare that, as required by these rules and conduct, I have fully cited and referred all material and results that are not original to this work.

Name: Md Rakim

Examination Roll Number: M4MEC22001

Registration Number: 131706 of 2015-16

Thesis Title: PHENOMENOLOGICAL MODELLING OF FLOW BEHAVIOUR OF ARMOUR STEEL MATERIAL AT ELEVATED TEMPERATURES WITH DIFFERENT STRAIN RATES

Signature: _____

(Md Rakim)

Dated: _____

FACULTY OF ENGINEERING AND TECHNOLOGY

JADAVPUR UNIVERSITY

KOLKATA -700032

CERTIFICATE OF APPROVAL*

This foregoing thesis is hereby approved as a credible study of an engineering subject carried out and presented in a manner satisfactory to warrant its acceptance as a prerequisite to the degree for which it has been submitted. It is understood that by this approval the undersigned do not endorse or approve any statement made, opinion expressed or conclusion drawn therein but approve the thesis only for the purpose for which it has been submitted.

Committee
On Final Examination for
Evaluation of the Thesis

Signature: _____
Date: _____
Seal:

Signature: _____
Date: _____
Seal:

*Only in case the thesis is approved

FACULTY OF ENGINEERING AND TECHNOLOGY

JADAVPUR UNIVERSITY

KOLKATA -700032

CERTIFICATE OF SUPERVISION

We hereby recommend that the thesis presented by Mr. Md Rakim entitled **"PHENOMENOLOGICAL MODELLING OF FLOW BEHAVIOUR OF ARMOUR STEEL MATERIAL AT ELEVATED TEMPERATURE WITH DIFFERENT STRAIN RATES"** was under our supervision and is accepted in partial fulfilment of the degree of Master of Mechanical Engineering.

_____

(Thesis Adviser)

Date: _____

Seal:

Countersigned by:

_____

(Head of the Department, Mechanical Engineering)

Date: _____

Seal:

_____

(Dean of Faculty of Engineering and Technology)

Date: _____

Seal:

ACKNOWLEDGEMENTS

"Work" is a definition of a joint endeavour that requires togetherness not only in respect of spreading our hands towards it but also the knowledge and experience builds its foundation. In this section, I am overwhelmed in all humbleness and gratefulness to acknowledge my depth to all those who have helped me to put these ideas, well above the level of simplicity and into something concrete.

I would like to express my gratitude to my supervisor Professor **Dr. Sanjib Kumar Acharyya** for his strong support, patience and constant availability for technical discussions. I feel motivated and encouraged by his technical discussions. I would like to express my particular gratitude to **Dr. Sankar Dhar** for being my well-wisher and rendering continuous support during my thesis work.

This thesis is the outcome of the kind co-operation, good-will, technical and beyond technical support extended by my seniors **Swagatam Paul, Mrinmoy Jana, Vaibhab Gangwar and Sukalpa Choudhury**. I am grateful to them for their suggestions in bringing this thesis into final form. Also, I would like to thank **Subhajit Ghosh** for his corporation and helping hand. It is great honour for me to have completed my thesis work in this group in such a good environment.

I am extremely thankful to all the faculty and staff of **Mechanical Engineering Department**.

Most of all, my deepest appreciation goes to **my Parents** for their faith, unyielding unconditional love, support, encouragement and quiet patience.

Abstract

Armour steels have a long history of providing optimal ballistic performance against a variety of battlefield threats, and they remain a cost-effective armour material. Armour steels are expected to not only improve, but also to continue to dominate vehicle armour designs well into the future. The properties of the material have been depicted well in this thesis that not only includes its physical properties but its chemical treatment. It also describes the material's different classifications into different categorized based properties.

In the present study a phenomenological constitutive model is developed to describe the flow behaviour of Rolled homogeneous armour (RHA) steel material at room to elevated temperature under different strain rates. A set of uniaxial tensile tests is done with the variation of strain rates and temperatures ranging from $10^{-4}\ s^{-1}$ to $10^{-1}\ s^{-1}$ and 25°C to 500°C respectively. From the experimental data, family of flow curves at different temperatures and strain rates are generated and fitted exponentially. The strain rate and temperature dependence of the coefficients of the exponential flow curves are extracted from these curves and characterised through a general phenomenological constitutive coupled equation. The coefficients of this coupled equation are obtained through average method.

ABAQUS is based on the finite element method and is classified as a general code applicable to both linear analysis and nonlinear simulations of single or multiphase problems. Finite element simulation of tensile tests at different strain rates and temperatures are done using the coupled equation in material model of Abaqus FEA software and validated with experimental results. Due to the unavailability of the preferable material model sub-routine in the Abaqus commercial package library that is needed here, a new user defined material model (UMAT) sub-routine is being developed here in this work.

As a step, material behaviour under different strain rate and temperature conditions is validated by comparing the simulation result with the test result graphically. For more confirmation in the validation part, the specimen is being changed from round and regular to flat complex geometry and the same uniaxial test has been carried out. Through graphical plotting, a vast comparison has been validated through simulation methods using normal simulation and by using damage parameter with it.

The novelties of proposed model are: (a) it can predict precisely the flow behaviour of tensile tests (b) it is a simple form of equation where fitting parameters are both function of strain rate ratio and temperature ratio, (c) it has ability to characterize flow behaviour with increasing elevated temperatures and increasing strain rates.

Keywords: Armour steel, RHA (Rolled homogeneous armour) steel, Phenomenological modelling, finite element simulation, User defined material model (UMAT).

Dedicated to My Mother, My Father and My Guide

Table Of Contents

Chapter 4

Chapter 5

Chapter 6

References

TABLE OF FIGURES

LIST OF TABLES

List of Symbols

Serial number	Symbol	Nomenclature
1	σ_f	Flow Stress
2	ε_e	Elastic Strain
3	ε_p	Plastic Strain
4	σ	Stress
5	$\dot{\varepsilon}$	Strain Rate
6	$\dot{\varepsilon}_0$	Reference Strain Rate
7	$\dot{\varepsilon}^*$	Non-Dimensional Strain Rate Ratio
8	T	Temperature
9	T_0	Reference Temperature
10	T^*	Non-Dimensional Temperature Ratio
11	E	Young's Modulus
12	G	Shear Modulus
13	σ_y	Yield Stress
14	σ_{ut}	Ultimate Stress
15	A, B, n	Material Constants

Chapter 1

1. Introduction

1.1 Background of the work

Protection has been the foremost criteria of defence where the world goes with the concept "Survival of the Fittest". Every living thing in our world seeks protection from its enemies. People have always tried to protect themselves from their enemies and the weapons they use, but this has always been counterbalanced by their need of mobility [1]. Protection causes a transformation in the soldier's internal paradigm, resulting in increased psychological endurance for moving freely in the battlefield, which causes a significant force multiplier impact. During any combat situation, protection is amongst the most important need for a soldier or in a fighting platform. Mother nature has developed a variety of protection mechanisms for all living things, most of which are yet unknown.

Among this, Armours are the most significant kind of protection. Armour would be the last line of defence and the closest thing to a soldier's heart on the battlefield. Armour has evolved over time as well, from the use of simple materials like leather to metals and more recently composites. The first armour was designed to protect the individual rather than any mode of transportation. The foot soldier was protected with a body vest, helmet, and shield since the Middle Ages. With the introduction of fire arms, the scale of attack was dramatically increased, and any form of protection was quickly abandoned in favour of the individual's increased mobility[1]. Soldiers may no longer be viewed as cannon fodder, so sufficient preparation and protection is needed.

There are several factors to consider when looking for the ideal armour material, but the most important factor is that the armour be effective. It must perform the function for which it was created [2]. Armour protection improves battlefield survival by a factor of ten. It enhances a soldier's morale and confidence, and acts as it's a big force multiplier. Furthermore, every soldier, his family, and his fellow citizens knows the consequence of the incident that occurs on the battlefield.

Steel has maintained its top position due to its low cost, dependability, availability of manufacturing infrastructure, concurrent value as a structural material, and ease of fabrication. Steels have long been used as armour because of its great strength, good hardness, and comparable lower cost than other armour materials. It has led to the development of various processing techniques like heat treatment and cold rolling that enhances the strength, toughness and hardness of steel which results in reduction of armour weight

Due to their high strength, hardness, and toughness properties, as well as their high energy absorption capability, armour steels are widely used as protective materials. They're mostly used in cast and rolled forms, and they're less expensive than newer armour materials like hybrid or reactive armours. Armour steels have a long history of providing optimal ballistic performance against a variety of battlefield threats and remain a cost-effective armour material.

According to Lt. Gen T.S. Shergill, today's casualties are a reason for concern and human life is seen as a very valuable commodity. As a result, we develop materials and modules that are

vital for the survival in future. The necessity of designing and testing new methodologies is needed to improve armour protection, even before firing a bullet for the development of a well-protected system.

Because it's difficult to achieve sufficient quench rates during heat treatment to achieve consistent and high hardness throughout thicker plates, armour steels come in a variety of thicknesses. As a result, material properties vary. This is seen with RHA, which comes in a variety of thicknesses (2.5 to 150 mm). To increase hardenability, thicker armour sections have a higher alloying content, but changes in composition cannot always fully compensate for such large changes in thickness, resulting in lowering hardness in the middle of the cross-section for thicker plates.

Nowadays, in war or politically unstable scenarios around the world, the combination of modern firearms and/or improvised explosive devices (IEDs) poses a high level of threat to both military and civilian targets. The current demand for armoured vehicles necessitates the development and improvement of armour materials such as metals, ceramics, and composite materials. Armour materials are used in both civil and military applications on land, sea, and in the air (examples in Fig. 1.1).

Fig. 1.1: Examples of land, marine and aerospace armoured vehicles

Vehicle operational requirements necessitate a constant trade-off between security and mobility. The current demand for armoured vehicles is for the armour mass to be reduced. Due to the need to produce lightweight vehicles, interest in using aluminium alloys for automotive body structures has grown. The high strength-to-weight ratio of aluminium is an advantage.

The goal of armour systems is to prevent projectiles from entering the protected region. Therefore, armour coated steel has become a global commodity for protection against explosives or ballistic projectiles and the steel industry is by no means exempt to technical innovations in the security sector. It is necessary to have a thorough understanding of the flow behaviour of an armoured structure in order to design it properly. Providing effective protection requires not only the development of ground-breaking materials, but also the precise definition of mechanical properties and the ability to implement them efficiently.

The flow curves of a material must be determined at various strain rates and temperatures in order to describe its flow behaviour. This property describes a material's ability to resist fracture in the presence of a crack, and it can be a function of plastic strain, strain rate, and temperature. However, because the specimen may not be in stress equilibrium, obtaining mechanical properties under dynamic conditions is quite difficult. Although some methods for specific cases have been proposed, there are currently no standards or guidelines for obtaining the flow curve of any material.

Today, a number of commercial finite element codes have been developed, with ANSYS and ABAQUS being two of the most popular. Both software packages can be used to solve problems ranging from simple linear analysis to advance nonlinear simulations, as well as problems involving component static, dynamic, thermal, and electrical responses. Because it excels at simulating explicit dynamic time-dependent problems, such as blast, impact, and fracture mechanics applications, ABAQUS has become a popular finite element platform for use in the fields of aeronautics and automotive engineering.

The need to improve design efficiency in industries such as automotive, aeronautical, and military has driven the development of material constitutive equations in the field of finite element modelling. Rusinek et al. (2009) [3] divides macroscopic constitutive modelling into two categories in their paper:

(I) **Phenomenological Constitutive Models**:

These models provide an empirically based definition of material flow stress, consisting of mathematical functions with no physical background that fit experimental observations. They have a small number of material constants and are simple to calibrate. They're only used in specific applications with a limited range of strain rate and temperature, and some materials have less flexibility. The Johnson-Cook Material Model [4] is an example of this type of constitutive model.

(II) **Physical-based Constitutive Models**:

These models, which are based on thermodynamics and kinetic slip and dislocation theory (e.g., Zerilli-Armstrong Model (1987); Feng & Bassims Model (1999), [5,6] account for the physical aspects of material behaviour. These models have a higher number of material constants, and their calculation procedure is based on physical assumptions. They better describe material behaviour under a wider range of loading conditions.

1.2 Development of strain rate-temperature dependent material model:

Following several years, Armour steel is the material that is mostly used for security measures for its properties like corrosion resistance at high temperatures, great strength, great hardness, excellent creep strength, low thermal neutron absorption cross section and great mechanical properties. This material is specifically used for optical ballistic performance which protects from the threats in battlefield and fragmentation because of its texture dependent tensile flow behaviour. So, it is necessary to construct constitutive equations for flow stress that uses finite element code for simulation in deforming materials during specific processes.

There are mainly two types of constitutive equations that defines flow stress which are (i) physical based and (ii) phenomenological (Y. C. Lin and Chen 2011) [7]. The physical based constitutive equations for flow stress are developed based on the observation of physical phenomenon of material deformation while the phenomenological constitutive equations for flow stress are constructed using empirical observations that are coined from the statistical mathematical tools.

Generally, the physical based equations are more accurate than the phenomenological equations regarding prediction of the flow stress behaviour. But the physical based equations consist large number of constants than the simple phenomenological constitutive equations for flow stress. Johnson-Cook (JC) [4], (Fu et al. 2016) [8], Modified Arrhenius (m-Arr) (Chen et al. 2019; Lei et al. 2019)[9,10], Khan-Huang (KH), Khan-Huang-Liang (KHL), Khan-Liang-Farrokh (KLF), Fields-Backofen (FB), and Molinari-Ravichandran (MR)[11–13] are the different types of phenomenological constitutive equations for flow stress. Examples based on physical constitutive equations for flow stress are Zerilli-Armstrong (ZA), modified Zerilli-Armstrong (m-ZA) Rusinek-Klepaczko (RK), Voyiadjis almasri (VA), Bodner-Partom (BP) and Cellular Automation (CA), Kocks–Mecking–Estrin (KME) (Seong et al. 2020) [5], [14–19].

Many research works have been taken into account regarding the two types of constitutive models constructed using different materials. Modified Johnson Cook model (m-JC), m-ZA, m-Arr and KHL models have been calibrated using Inconel 625 super alloy for investigating the effect of strain rate and temperature on flow stress and it has been summarized that the m-Arr is the more appropriate one (Badrish et al. 2020) [20]. Arrhenius-type equation are used for the prediction of the flow stress behaviour of Aluminum alloy 7A04 when the material is focused to isothermal compression test at high temperatures, and the conclusion is drawn in good agreement with the experimental data (Qiang et al. 2020) [21]. Predictions regarding the flow stress for uniaxial isothermal and dynamic compression tests at ranges from 673K to 1373K has been investigated with m-ZA, Cowper Symonds (CS), m-JC, Arr, KHL and the m-JC has been reported as the suitable model (Saxena et al. 2019) [22]. Various types of Arrhenius-type constitutive models have been taken into consideration for predicting tensile behaviour of 17-PH stainless steel sheet and of getting accurate prediction has been recorded through multi-strain modified models (Su et al. 2020) [23].

In a contrast study on predicting the accuracy of m-ZA and m-JC for isothermal deformation of Aluminum 5083 + SiC composite, the m-ZA has been observed as the better matched model than the latter (Rudra, Das, and Dasgupta 2019) [24]. JC, m-JC, FB, KHL and Mechanical Threshold Stress (MTS) constitutive equations for flow stress have been used for Ti-6Al-4V alloy for low strain rates and for high temperatures. Their predicting capabilities also have been

differentiated along with their statistical parameters in ref. (Kotkunde et al. 2014; Tao et al. 2018) [13,25]. The flow stress behaviour of friction welding of GH4169 super alloy has been recorded using the m-FB, JC and Arr models. The experimental data on stress has been in good terms with the predicted stress through Arr (Geng et al. 2018) [26]. Experimental compressive stress of Al-Zn-Mg-Cu Aluminium alloy at high temperatures has been contrasted with the predicted stress through Arrhenius type equation, and it has been summarized with high coefficient of correlation (R) of 0.993 (Zhang et al. 2018) [27].

The hyperbolic-sine Arrhenius equation has been used for the prediction of hot compression stress between two different Titanium alloys and the prediction capability of the model also has been improved by decreasing the gradient refinement method (Bodunrin 2020) [28]. Likewise, JC, m-ZA, m-Arr also has been calibrated for the austenitic stainless steel 316 at the temperature ranges between 323-623K and strain rate ranges between 0.05-0.3 (Gupta, Anirudh, and Singh 2013) [29]. Moreover, the hot deformation behaviour of 7055 Aluminium alloy is investigated using the phenomenological models: J-C, modified Fields-Backofen (m-FB), Arrhenius (Arr)[4][26,29]. It has been concluded that the Arr predicts accurately by taking into consideration the strain rate – temperature combined effect (Wang et al. 2018) [30].

In addition, with that, the JC model [4] and ZA models [5] have been reported for accurate predicting the flow stress for Ti-6Al-4V alloy at high strain rate and for elevated temperatures (Che et al. 2018) [27]. FB, Fields-Backofen-Zhang (FBZ) and modified Field-Backofen-Zhang (m-FBZ) [31] have been used for the prediction of the isothermal tensile flow stress in alpha-Ti tubes. From the three, m-FBZ model prediction is more accurate with R value of 0.9873 (Y. Lin et al. 2018) [32]. JC, m-JC models have been used to predict flow stress of Al7075 at elevated temperatures and as the modification of temperature term in JC, the m-JC has given better prediction (Rasaee, Mirzaei, and Almasi 2020) [33].

Comparison between the constitutive relations with the experimental results is described as the functional form of strain rate and temperature. It has been proposed from the constitutive relation described by Johnson-Cook [4], the modelling of material behaviour dependence on strain rate and temperature, basically for steel. For same ranges of strain rate, the rate sensitivity cannot be correctly predicted from the research of Zhao and Gary (1996) [34,35] as well as from the Johnson-Cook relationship. In fact, from the proposed relationship stated by Zhao and Gary (1996) [34,35] we cannot determine strain hardening from the effects of the strain rate and temperature. The original version of the Johnson-Cook [4] relation which is directly proportional to the effect of linear rate in logarithmic scale is more complicated to solve, by taking into consideration as constant (C) that disagrees with the experimental observations.

In due course of time, to correct this problem, some authors have coined a complementary term with the part of strain rate expression of Johnson-Cook relation (Peixhino et al., 2003) [36]. Still the problem exists with high strain rates, when temperature rises that results thermal softening of material caused due to adiabatic heating, the resultant effect is not well defined by the relation of Johnson and Cook (1983) [4]. The failure appears easily with the Johnson-Cook approximation, if we define failure of structure using energy criterion, neglecting the mechanical resistance of the structure. The effect of this study on DP 600 steel was investigated by Rusinek et al. (2007) [37]. In the RK constitutive relation, a possibility was taken into consideration that with the jump of ascending or descending strain rates, a subsequent advantage is observed. Through experiment by Klepaczko and Duffy (1982) [38] the behaviour was observed for BCC metals which is subjected to strain rate jump at a particular plastic strain

that is characterized by an increase of stress with comparison to the actual stress level at the persisting strain rate that to some extent was modelled by the RK [14] relation. Such behaviour was demonstrated by a microstructure evolution.

For the study of physics of plastic deformation (thermal activation, dislocations, etc.) models like physically based and internal variable are proposed. Both the models have succeeded in fitting the experimental data that is available for a particular range of strain, strain rates and temperatures. In addition to this, both the models have limited success in understanding the available constitutive data for a great range of strain rates or rather more accurately predicting stress change for quick changes in strain rate (e.g., Follansbee and Kocks, 1988) [39]. Many models of this type also cannot properly explain in satisfactory way, for example in copper, the dependence of strain rate on strain hardening (Tong et al., 1992; Bodner and Rubin, 1994) [40,41] and at high temperature the strengthening with the usage of high strain rate deformation (Frutschy and Clifton, 1998) [42,43].

In current years, it has also been observed that in modelling, substantial development happened for the physics of deformation in plastic as well as for the stress dependence on the parameters in microscopic aspect such as the dislocation density, cell size and mis-orientation of cells. To observe and explain strain hardening for various stages the above models have was developed for large strain metal deformation (e.g., Nes, 1998) [44]. Current development in modelling of materials for macroscopic behaviour of materials basically focused on the sub-structure evolution and its incorporating effects (Vander Giessen and Needleman, 1995; Ortiz and Repetto, 1999; McDowell, 2000; Ashmawi and Zikry, 2003) 45–47]. Many research teams have observed this considering over a numerous range of strain rates and temperatures for wide range of metals like FCC (aluminium, copper, nickel) and BCC (a-iron, chromium, niobium).

There are several researchers who worked for finding constitutive modelling of flow stress behaviour of a material at a different strain rates and temperatures. Some of famous and useful constitutive models are described below:

G.R Johnson and W.H. Cook [4]**:** A constitutive model and data for materials exposed to large strains, high strain rates, and high temperatures are presented in this study. Torsion tests across a wide variety of strain rates, static tensile tests, dynamic Hopkinson bar tensile tests, and Hopkinson bar teats at elevated temperatures provide the data for the material constants. Although there are some reservations about this aspect, the model works well for a variety of materials, including ferrite, copper alloy, Carbide brass, and Nickel 200. Because it includes variables that are readily available in most of the applicable computer software, the basic form of the model is well suited for calculations. When strain hardening does not increase as strain rate increases, this is a basic empirical model that is not always appropriate.

S. R. Bodner and Y. Partom [16]**:** A set of constitutive equations has been formulated to represent elastic-visco-plastic strain-hardening material behavior for large deformations and arbitrary loading histories. At all phases of loading and unloading, the total deformation rate is thought to be separable into elastic and inelastic components that are functions of state variables. As a result, the theory is unaffected by a yield criterion or loading or reloading conditions. Material constants were used to reflect commercially pure titanium in the computations. This model has the drawback of being unable to account for the temperature effect.

Frank J. Zerilli and Ronald W. Armstrong [5]**:** Strain hardening, strain-rate hardening, and heat softening effects have been combined into a very accurate constitutive model for copper. The relationship has a straightforward expression and should be applicable to a wide range of FCC materials, as well as the influence of grain size. There is no better description of the impact of deformation twinning in BCC materials. At high temperature effect zones and very high strain rates, the Zerilli-Armstrong model is unable to predict a satisfactory temperature impact.

Rusinek, R. Zaera and J.R. Klepaczko [37]**:** The model is based to some part on Klepaczko's earlier concept of physical modelling. Strain hardening, strain rate, and temperature sensitivity are all included. A thermos-visco-plastic algorithm which is based on the J2 theory of plasticity is built to implement the RK constitutive relation. The biggest drawback of this concept is that it cannot be applied in more than 100°C.

Molinari and G. Ravichandran [48]**:** To characterise the behaviour of metals under a wide variety of loading situations, a phenomenological constitutive model is proposed. The model is composed of a single internal parameter that may be considered as being connected to the microstructure that emerges in the metal after deformation on a specific length scale. The constitutive model is demonstrated by examining copper's reaction and comparing it to existing experimental data over a wide range of strain rates and temperatures. Pure OFHC copper is the only material for which the model's application and efficacy are limited.

Nemat-Nasser et al. (1994), Nemat-Nasser and Isaacs (1996) [49,50]**:** Nemat-Nasser et al. (1994), Nemat-Nasser and Isaacs (1996) performed a high strain-rate recovery test, which they utilised to investigate tantalum's thermal softening behaviour under high strain-rate deformation. According to their results, due to the combined effects of strain and strain-rate hardening, the effect of thermal softening at high strain deformation for tantalum dominated the work-hardening behaviour.

Akhtar S. Khan and Riqiang Liang [51]**:** The constitutive model is based on a strain-rate jump test in which a specimen was deformed and then jumped to some step interval to a strain rate of $2450s^{-1}$. After that, the specimen was machined from the deformed specimen and the dynamic test was done using SHPB technique. The strain data used in the constitutive model were the experimental data. In quasi-static test, the strain rate data was calculated from the actual strain-time history data. A dynamic test for the deformed specimen was also carried out using SHPB technique after the quasi-static test to a strain rate $2490s^{-1}$. The constitutive model predicted the material response during strain-rate jump tests quite well in this case too.

J.A. Rodríguez-Martínez et al. [52]**:** A constitutive description for modelling the behaviour of FCC metals has been developed. It assumes the plastic flow decomposed into internal stress and effective stress. The internal stress represents the applied stress required for the transmission of plastic flow between the polycrystalline grains. The effective stress formulation, which is the main innovative feature of this work, represents the thermally activated deformation behaviour. This is defined taking into account the inter-relationship between strain rate and temperature, and gathers structural evolution dependence.

J. Richeton et al. [53]**:** The paper presents experimental results illustrating the effect of strain rate and temperature on the mechanical response for three amorphous polymers (PC, PMMA and PAI) under a wide range of strain rates and temperatures. PC, PMMA and PAI are amorphous polymers widely used for their optical and mechanical properties. The aim of this

article is to model the compressive yield stresses according to the new formulation of the Eyeing cooperative model as proposed by Richeton et al. (2005). At the end, J. Richeton et al. discuss how the effect of hydrostatic pressure can be incorporated in the proposed model.

Nemat-Nassera et al. [54]**:** In this paper, uniaxial compression tests are performed on cylindrical samples to understand and model the thermo-mechanical response of AL-6XN stainless steel. True strains exceeding 40% are observed in these tests, over the range of strain rates from 0.001 s^{-1} to about 8000s^{-1}. A physically based model for the behaviour of this material has been developed. The microstructure of the undeformed and deformed samples is observed by optical microscopy. Model predictions are compared with the results of the experiments. Good agreement between the theoretical predictions and experimental results is obtained.

Miguel Ruiz de Sottoa et al. [55]**:** A constitutive model has been developed accounting for the combined effect of plastic orthotropic and tension/compression asymmetry, strain hardening, strain rate hardening and thermal softening. Aircraft fan blades are designed to withstand impact loading involving large deformation, high strain rate, non-proportional loading paths and self-heating. An extensive experimental campaign on a Ti-6Al-4V titanium alloy provided in the form of cold rolled plates has been carried out. The performances of the model have been estimated by conducting numerical simulations.

A. Banerjee et al. [56]**:** In this paper, the behaviour of standard armour steel materials at large strains, high strain rates, and high temperatures. To reflect the strain rate sensitivity of metals, Johnson and Cook (J–C) constructed an empirical constitutive relation. Some changes to the J–C damage model have been proposed, as well as a simulation of three separate tensile tests on armour steel specimens and found good matching with the experimental results.

A. Uenishi and C. Teodosiu [57]**:** The work hardening behaviour of IF steel is investigated using a physically based modelling and experimental approach that covers a wide range of strain rates. The research shows that the apparent excess of flow stress following a change in strain rate, which is common in bcc metals, is really due to thermal softening at large stresses. Through the strain-rate dependent development of dislocation structures, the strain rate impacts not only the short-range but also the long-range stress. This model is only applicable to obtain an isothermal stress-strain curve at high strain rate.

Dipti Samantaray et al.[58]**:** A modified constitutive model based on the Zerilli–Armstrong model has been proposed for considering the effects of thermal softening, strain rate hardening and isotropic hardening. This has been attributed to the inadequacy of the JC model to incorporate the coupled effects of strain and temperature and of strain rate and temperature. Data from isothermal hot compression tests over a wide range of temperatures (1073–1473 K), strains (0.1–0.5) and strain rates were employed to formulate a suitable model.

Haidong Yu et al. [59]**:** In this work, the experiment is done on the uniaxial tensile test for different strain rate range (0.0001 to 1600 s^{-1}) in DP600 steel to capture the effect of strain rate on flow behaviour and yield phenomenon of the materials. For simulation, Johnson-Cook material model is used for the stress strain curve and the results was found in good agreement with experiment results.

R. Matadi Boumbimba et al.[60]**:** In this paper, high strain rate compressive yield stress of polypropylene based organoclay Nano composites has been studied. A proposed approach

accounts for strain rate and temperature effects as well as for the extent of exfoliation of the organoclay fillers. It is based on the cooperative model for the yield behaviour of semi-crystalline polymers. Split Hopkinson pressure bars apparatus was used to carry out high strain rate tests at various temperatures and strain rates.

Surajit Kumar Paul (2012) [61]**:** To characterise the flow behaviour of metals over a wide range of strain rates and temperatures, a phenomenological constitutive model is used. In different strain rates and temperatures, the suggested model is used to predict yield stress and flow curve form. The determination of eight material constants for the proposed model using experimental data is straightforward and simple. For various steels (mild steel ES, DP600 and TRIP700), model predictions demonstrate a high level of agreement with experimental data.

Surajit Kumar Paul et al. [62]**:** The tensile properties of low carbon, ultra-low carbon, and micro alloyed steel sheets under low to intermediate strain rates are the subject of the study. Under intermediate strain rate deformation, experimental investigation reveals two essential properties of these steels. To begin with, the yield stress in all of these materials increases as the strain rate increases. Consequently, the yield stress increment is bigger for low carbon steel sheets. Second, as the strain rate is raised, the rate of strain hardening falls dramatically. Based on these results, a constitutive model has been constructed that predicts all of these classes' strain rate sensitive flow behaviour.

Woei-Shyan Lee and Chen-Yang Liu [63]**:** Microstructures of the impacted specimens are studied using a transmission electron microscope (TEM). It is found that an increased carbon content enhances the dynamic flow resistance of the three steels. A thermal softening effect is also found in the plastic behaviour of the S15C low carbon steel, S50C medium carbon steel and SKS93 high carbon steel. The activation energy (G*), varies as a function of the strain rate and temperature, but is apparently insensitive to the carbon content level. Flow stress increases with strain and strain rate in every case. The errors between the calculated stress and the measured stress are found to be less than 5%. The current results provide a valuable reference for the application of these steels in high-speed plastic forming processes.

Swagatam Paul et al.[64]**:** A phenomenological constitutive model has been developed to describe the flow behaviour of 20MnMoNi55 low carbon reactor pressure vessel (RPV) steel at sub-zero temperature. The strain rate and temperature dependence of the coefficients of the exponential flow curves are extracted from these curves and characterised through a general phenomenological coupled equation. A genetic method is used to optimise the coefficients of this coupled equation. Abaqus FEA software is used to perform finite element simulations of tensile testing at various strain rates and temperatures.

Practical applications require knowledge about plastic response for large deformations as well as at high temperatures and strain rates. For example, process like metal forming and its impact or penetration problem together combines the effects of large strain, high strain rate and temperature. For good constitutive description, the material modelling of such processes should be accurate in behavioural aspect [65].

For the present modelling, the relationship is not direct to the evolution in microstructural aspect but it is similar to that as the adiabatic heating that creates similar phenomenon. Hence, for materials with metallic nature of BCC microstructures such as mild steel, the necessity to introduce a more complicated physical modelling is less but the introduction of a more

particular approximation of strain hardening coupled with temperature and strain rate is sufficient. This is not at all for FCC materials with metallic nature, the microstructure evolution effects at different strain rates are much more important.

Though the existing material models are suitable for elevated temperatures and strain rates but it cannot be applicable in case of armour steel material with elevated temperatures. In this work, an attempted has been taken to developed a constitutive model which predicts flow stress at elevated temperatures and high strain rates that are appropriate for the armour steel material [66]. Generally, two types of approaches are available in literature for the development of a constitutive model based on flow stress considering temperature, strain rate and plastic strain as a function form [65]. Some group of researchers approves flow stress as a function of temperature, strain rate and plastic strain [5,16] whereas the latter half takes into consideration the rate of strain hardening as a function of temperature, strain rate and plastic strain [37,48,49].

In this work the first approach is taken into account where flow stress is considered as a function of temperature, strain rate and plastic strain. The experimental flow curve is fitted with suitable function for each temperature and strain rate. Then the constants of the fitting curve are plotted with the variation of temperatures and strain rates. A constitutive equation of flow stress is proposed where the temperature and strain rate are in a coupled from. To obtain the optimum value of the coefficients of the constitutive equation, average method is considered. Lastly, a free form equation is developed and FE simulation of tensile test at each temperature and strain rate is done using the developed constitutive equation as an input for material.

Although the present modelling is phenomenological in nature because these models provide an empirically based definition of material flow stress, consisting of mathematical functions with no physical background that fit experimental observations. The predicted results of the constitutive model are described in the present model and comparison is made with the experimental results for armour steel materials for a wide range of strain rates and elevated temperatures.

1.3 Motivation of the thesis work:

From the literature review it can be reported that the phenomenon of flow stress in a material can be extracted using phenomenological model methodology. But the application of phenomenological model is case sensitive because of the dependence on plastic strain, strain rate and temperature conditions. That's why, the development of phenomenological model at different loading condition (temperature and strain rate) is crucial for our particular grade of armour steel material.

From the literature, it can be observed that material grade of specimen and loading conditions (temperature and strain rate) has some constructive effect on flow stress phenomenon. So, effect of geometry and loading condition (temperature and strain rate) is also a concerning point that should be considered for our particular armour steel material. For the application of the phenomenological model methodology for analysing in the component level, finite element method is the requirement. In literatures, there are numerous material models that are available to capture the effect of strain rate and temperature. But for elevated temperature regime, a perfectly fit strain rate temperature sensitive material model is needed to be constructed for our particular Rolled Homogeneous Armour (RHA) material.

1.4 Objective of the present work:

1. To study the effect of strain rate on tensile properties (Yield Stress, Ultimate Stress, Young's modulus), for that a series of tensile tests are conducted at room and elevated temperature in different strain rates ($0.0001s^{-1}$, $0.001s^{-1}$, $0.01s^{-1}$, $0.1s^{-1}$) according to ASTM E8 standard.
2. To study the effect of temperature on tensile properties (Yield Stress, Ultimate Stress, Young's modulus), for that a series of tensile tests are conducted at different strain rates in different temperature (25°C ,200°C, 300°C, 400°C, 500°C) according to ASTM E8 standard.
3. To develop phenomenological material model that is sensitive to elevated temperatures and strain rates for the flow behaviour obtained from tensile tests.
4. To check the effectiveness of material model over simple elastic-plastic material using Finite element analysis of tensile testing.
5. To validate the application of material model for different strain rates, temperatures and different geometrical shape of the specimen. And also, to validate the finite element simulation results with experimental tensile results of flow curve at these conditions.

Chapter 2

2. Brief overview of the material with experimental details

2.1 Material:

Armour steel is a high-strength, low-alloy structural steel that has been processed to provide extremely high penetration resistance. This feature is commonly imparted to steel by heat treatment, usually through thermo-mechanical treatment. It is commonly known that raising the texture intensity of steel, which may be achieved by thermo-mechanical treatment, can enhance its resistance to penetration. The armour's mass effectiveness rises as the material's hardness rises. Hard armour, on the other hand, is brittle and prone to shattering when struck.

The chemical composition, austenitization and tempering temperatures, and grain size of steel all have an impact on its mechanical properties, characteristics and, as a result, its ballistic performance. It has also been proven that altering the chemical composition and heat treatment parameters may improve the mechanical characteristics and ballistic effectiveness of martensitic steels.

Quenching and tempering, which is described as the heating and cooling of a metal or alloy, alters the microstructure of the steel and enhances the strength, hardness, and toughness of the treated materials. During the quenching of austenitic steel, the cooling rate should be such that the steel cools down below the martensite formation temperature. After the steel's whole microstructure has been transformed to martensite, the martensite is tempered.

The temperature of the steel is increased during the tempering process to a point where martensitic structure of such steel can be tempered. The finish rolling temperatures and quenching and tempering rates must be managed during the hot rolling of the plate during the quenching and tempering process in order to get the best quality steel grades with low alloy content. The resulting low alloy quenched and tempered steel products provide designers of armoured vehicles with strength-to-weight benefits and wear-resistant qualities not seen in ordinary steels.

Armour plate production requires cutting-edge technologies. Because high-strength, high-hardness steels are required, among the most severe process approaches is required for steel plate manufacture. Armour steel can be made in a basic oxygen furnace (BOF) or an electric arc furnace (EAF).

Nickel (Ni), chromium (Cr), and molybdenum (Mo) are the major alloying elements in armour steel (Mo). This steel's sulphur (S) and phosphorus (P) content must be extremely low (preferably less than 0.015 percent of each element). In addition, the dissolved gases nitrogen (N_2), oxygen (O_2), and hydrogen (H_2) have relatively low values in this steel. Furthermore, the steel must be extremely smooth, with very few inclusions.

2.1.1 Classification of armour steel:

Due to the different alloying element and production procedure armour steel can be classified into four main groups. These groups are:

(i) Rolled homogeneous armour (RHA),
(ii) High hardness armour (HHA),
(iii) Variable hardness steel armour (VHA) and
(iv) Perforated armour (PA).

(i) Rolled homogeneous armour (RHA):

Among these four groups, rolled homogeneous armour (RHA) steels are usually recognised as a benchmark material. For a long time, RHA steel has been considered the standard armour for light armoured vehicles. It has a high-quality alloy steel that's rolled out before being heat treated to provide the highest strength, hardness, and toughness that can be possible.

Most of today's combat tanks, rolled homogeneous armour (RHA) steel remains as the standard armour material. After heat treatment, this amour steel is utilised in the tempered martensitic microstructure, which entails hardening to raise resistance to projectile penetration and then tempering to make it harder and therefore improve the energy absorption capabilities against impacting projectiles.

(ii) High hardness armour (HHA):

Another most popular armour steels are high-hardness armour steels (HHA). The HHA steels are must be flexible, weldable, and fatigue resistant. Normally, they are used utilised as load-bearing construction steels. HHA steel typically has a carbon content of 0.27 percent. The microstructure of the heat-affected zone is a function of the cooling rate imposed by the welding process and the chemical composition of the base plate. Material hardness is strongly dependent on the welding temperature history. So, High-hardness armour (HHA) steel requires careful control of the welding procedure.

(iii) Variable hardness armour steel (VHA):

Variable hardness armour steel (VHA) is made by rolling a high hardness front plate to a reduced hardness back plate, commonly known as dual hardness armour (DHA). To increase impact resistance, "dual-hardness" armour plate, which consists of a hard but brittle outer layer connected to a tough but flexible inner or base layer, has recently been used. The hard outer layer offers a resistive barrier to the impacting component and prevents the underlying ductile material from penetration, whereas the ductile base layer supports the outer brittle material and prevents it from brittle fracture.

At the moment, dual-hardness armour plates are made by rolling two flat plates together, each with the necessary properties. The ultimate result is a dual-hardness flat plate that is produced into the required shape. VHA steels that are roll-bonded are difficult to manufacture and have recognised manufacturing constraints. Electro-slag re-melting methods have been studied as a means of creating VHA steels, but the process remains problematic.

(iv) Perforated armour (PA):

For many years, high-strength steel perforated plates have been used in armour systems to increase ballistic performance by introducing varied shaped combinations. The holes or slits of perforated plate armour are generally designed to interact with threat's diameter, and the performance of such armour is dictated by the material's strength, plate thickness, and whole orientation. Each hole can have the same or different shape that can be in form of slits, and are arranged in a regular or irregular pattern. When a bullet strikes the side of a hole in perforated plate armour, bending force is created, which breaks the approaching projectile core or diverts the projectile off its incidence trajectory, reducing penetrating capacity.

Perforated armour works by causing the bullet to be disrupted and twist, reducing the armour penetrating potential. Making the perforations can be expensive since they must be done either before or after the armour is hardened and they must be done in such a way that the material does not heat up and lose its hardness.

2.1.2 Properties of armour steel material:

(a) Hardness:

Hardness is a predicted strength measurement that may be easily assessed on a plate-by-plate basis, and it's especially useful as a quality assurance performance. The armour's mass effectiveness raises as the material's hardness rises. Hard armour on the other hand, is brittle and prone to shattering when struck. Higher resistance to plastic flow in a ductile hole formation failure mechanism causes the first improvements that come with increased plate hardness.

Greater plate hardness, however, beyond a certain point, leads in poorer protection owing to the material's increased sensitivity to low energy adiabatic shear failure, which results in addition to increase in plate hardness, however, it results with higher performance, but only as a result of projectile fracture. Depending on the exact steel hit, a lack of toughness at very high hardness levels might result in brittle failure of the steel plate and hence unpredictable behavior [67].

(b) Strength:

Armour steel is a high-strength, low alloy structural steel that has been processed to provide extremely high penetration resistance. The thermo-mechanical treatment generally imparts this feature to the steel. It is commonly known that raising the texture intensity of steel, which may be achieved by thermo-mechanical treatment, can enhance its resistance to penetration.

High strength materials, such as armour steel, small local plastic zones (and hence extremely high local stresses) are frequently seen in front of cracks. Even when external forces are minimal, a significant local stress can be generated, leading to fast micro-crack propagation and fracture [68].

(c) Toughness:

The toughness of armour steel is substantially stronger in the plate transverse and longitudinal direction than in the short transverse (through thickness) direction. This is due to alloying element segregation during the casting process, notably Sulphur-based non-metallic inclusions, as well as orthotropic microstructure deformation during the rolling process. The failure mechanism and ballistic resistance of a tempered and quenched steel changed depending on the orientation of the micro-structural banding in the plate, according to Leach and Woodward [69].

(d) Fatigue Strength:

While fatigue strength is feasible in armour steels, it is uncommon in practise since armoured structures are often overdesigned from a fatigue standpoint. Fatigue is usually linked to inadequate weld joint design, which results in complicated residual stresses under dynamic loads which are either unanticipated non-design loads or persist over a longer time than a reasonable service life.

(e) Structural Cracking:

When cracking occurs fast or propagates through with an armour plate to the point that the local structure has been unable to withstand any more structural or impact loads, the armour structure is said to be fail. The prevention of cracking, also known as structural cracking, is critical to the structural integrity and ballistic integrity of armour steels. Suitable armour selection and manufacture will prevent, of structural cracking, resulting in costly structural remedial repairs.

(f) Corrosion Resistance:

Corrosion resistance is a type of cracking that is helped by the environment. High-strength armour steels, for example, have been demonstrated to be substantially more prone to cracking in saltwater than in other conditions, even tropical ones [66]. Following crack initiation, stress corrosion cracking occurs when all three of the following criteria are present: (I) An applied or residual stress, (II) A susceptible microstructure and (III) A corrosive environment.

(g) Penetration and ballistic resistance:

The ballistic performance and penetration mode of armour steel are said to be directly determined by its high hardness. Hardness and perforation resistance, as defined by the protective ballistic limit, do not have a fundamental relationship. To increase the ballistic performance of armour steels, research on alloying design and heat treatment condition is highly common.

(h) Ductility:

Ductility is assessed in a uniaxial tensile test by the fracture strain, which accounts for both homogeneous and necking strain once the ultimate tensile strength is attained. Ductility is a uniaxial measurement of the total elastic and plastic strain in a ductile material before micro-void development, growth, and coalescence, which leads to ultimate fracture.

When the ductility of an armour plate is inadequate to sustain the forces associated with bending originating from an impact, and bending is the chosen failure mode, shattering of the armour plate might occur [70].

(i) Adiabatic Shear:

Zener and Hollomon [71] proposed the general theory of adiabatic shear by deriving a maximum shearing strain rate from thermo-mechanical material parameter. Recht [72] extended the theory to provide a relative ranking of materials with respect of their sensitivity to adiabatic shear. Low thermal conductivity, specific heat, density and work hardening rate as well as high shear yield stress and thermal softening rate, were favorable to adiabatic shear.

Adiabatic shear is a critical failure mechanism for high-strength armour steels because it produces low energy failure mechanisms throughout a wide range of hardness values, where diminished ballistic performance is common. Despite the fact that considerable study has been done over the years, adiabatic shear will remain a significant research area for so many years to come.

(j) Fabricability:

Cutting, forming, welding and machining are all examples of fabrication procedures. It is well known that specific metallurgical characteristic of armour steels is required for fabrication activities. The major property criteria for production of armoured steels are low carbon equivalent (CE), minimal segregation, low hydrogen content, low residual stress and good ductility.

(k) Thermal properties of armour steel:

In general, quenching and tempering are well-established methods for producing armour steel strengthening while keeping or even improving impact toughness. In steels, martensite has the highest level of strength in all the structures created by heat treatment. The martensite phase, on the other hand, is rarely employed in its natural state due to the high internal pressures involved with the martensite transition. Tempering improves ductility and toughness, both of which are important for impact energy absorption. In steel, the tempered martensite lath structure also delivers the best dynamic strength [73].

2.1.3 RHA Armour steel:

The armour material under study is a medium carbon, low alloy steel with chemical composition given in table 2.1. The test sample of this material is received from Bhabha Atomic Research Centre, India. This material satisfies the requirements of armour plates that are used as protective cover of a particular class of battle tanks (MBTs), infantry combat vehicles (ICVs), light vehicles, helicopters and body armour have all been conceived, manufactured, and deployed in this manner. So, the goal of armour systems is to prevent projectiles from entering the protected region. In a steel plant, the cast material in the form of ingots was rolled over a number of steps into plates with desired thickness. Thereafter, the plates were soft annealed, shot-blasted and cut to desired size. The plates were then suitably heat treated to develop a tempered martensite microstructure. This gave an ideal combination of hardness, toughness and strength of the material. The heat treatment schedule followed for the armour steel plates is shown in the fig. 2.2.

Table 2.1: Chemical composition of RHA armour steel in percentage

C	Si	Mn	P	S	Cr	Mo	Ni	V	Al	Fe
0.31	0.14	0.43	0.011	0.005	1.41	0.42	1.57	0.08	0.04	Rest

Fig.2.3 shows the microstructure of the armour steel material. It depicts uniformly distributed tempered martensite with no ferrite grain boundary. Absence of ferrite network indicates proper heat treatment. Absence of banding or segregation shows that homogeneous is adequate. Specks of white areas seen in the microstructure are retained austenite.

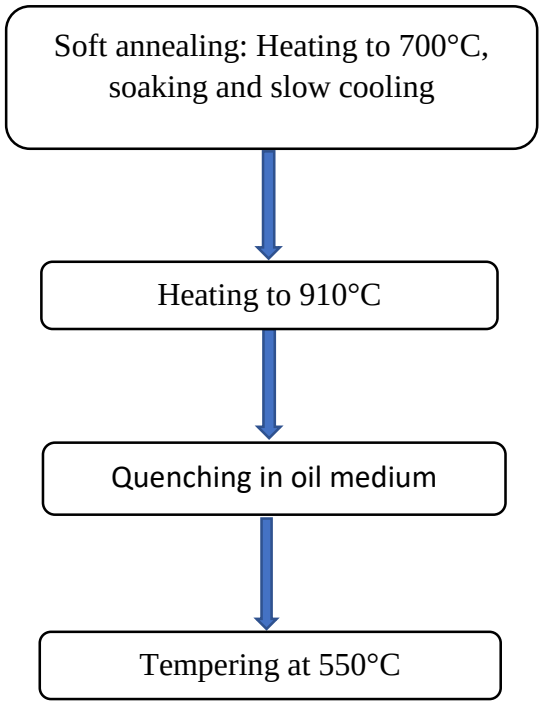

Figure 2.2: Heat treatment schedule of RHA armour steel plate

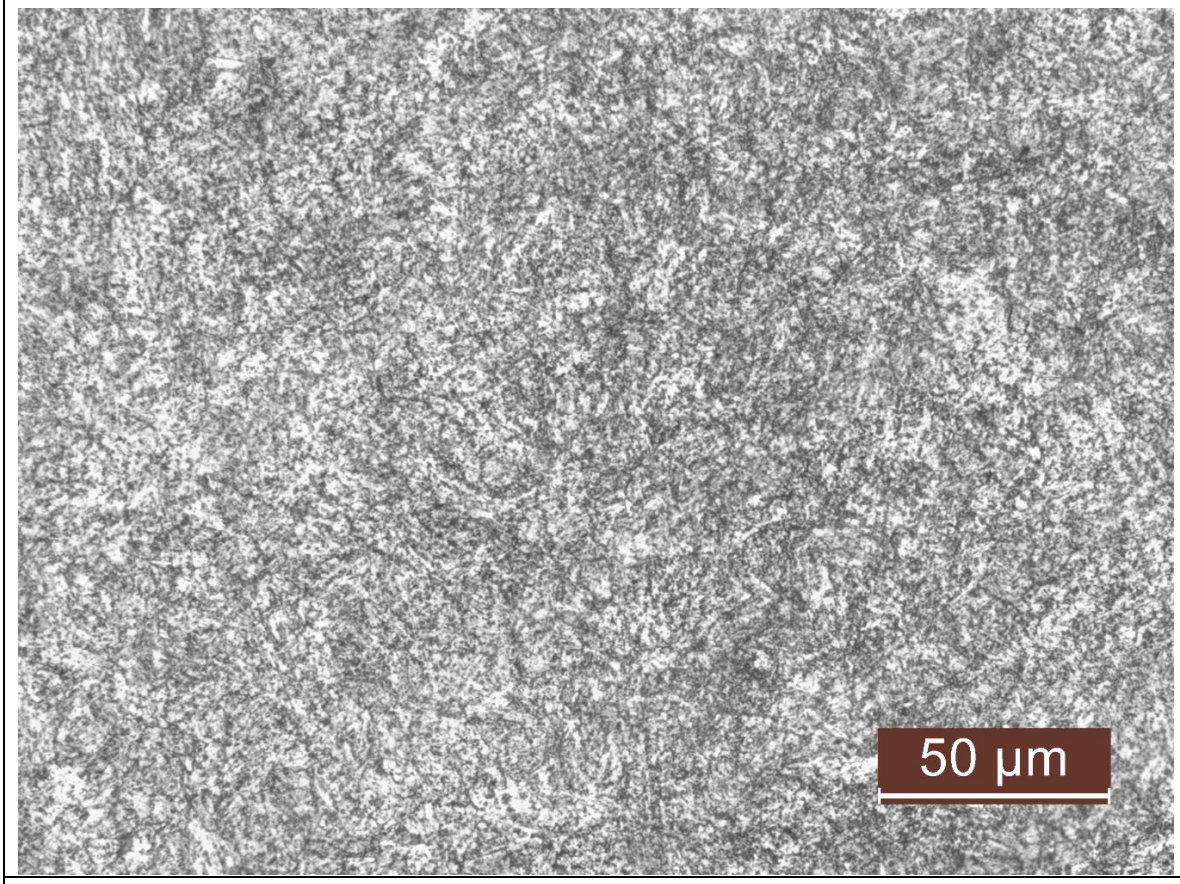

Fig. 2.3: Microstructure of RHA armour steel material

2.2 Details of the experiments:

2.2.1 Experimental procedure of tensile test:

According to the standard procedure of ASTM E8 in Instron 5582, (electro-mechanical machine) all the tests of uniaxial tensile are done. The machine capacity is 100 KN and the coil is being heated to achieve rise in temperatures during test. Five different temperatures (25°C, 200°C, 300°C, 400°C, and 500°C) and four different strain rates ($0.0001s^{-1}$, $0.001s^{-1}$, $0.01s^{-1}$ and $0.1s^{-1}$) are used for the test in the present work.

Before conduction of the tests, the length and diameter of the gauge for all the specimens under test are measured and are provided to the data acquisition system for stress and strain measurement. The top surfaces and bottom ends of all the specimen are clamped in between the static grips of the alignment. All the dimensions of the test specimen are shown in Fig. 2.6 and the detailed test matrix shown in the table 2.2.

The usage of Dynamic extensometer is to get the value of the strain at uniform cross-section part of the specimen to be used. The Dynamic extensometer gauge length is 25 mm and the travel is ±3 mm. All the tests are done in displacement control mode and different displacement rates or velocities are used as an input. After that, the calculations are done for strain rates from specimen's gauge length and its corresponding velocities. For every specimen, on an average of 30 minutes thermal soaking time is used to acquire uniform temperature throughout the body.

Fig.2.4: Instron 5582, Electro-mechanical machine	**Fig.2.5:** Instron 5582 Temperature Controller

The load cell that is fixed above the upper grip is used to measure the load of the test specimen line. Linear Variable Differential Transducer (LVDT) is used to measure the actuator stroke position. As the desired speed is acquired by the actuator, the spacer rod knocks out the wedge, which is pre-set for the requirement of the test. The pre-tension bolts grip the specimen between the moving grips and the actuator continues to move till the failure of the specimen.

Table 2.2: A summary of test matrix

Specimen no.	Test Temperature (°C)	Strain Rate (s^{-1})	Gauge length (mm)	Gauge Diameter (mm)
1	25	0.0001	37.80	5.94
2		0.001	36.91	5.98
3		0.01	41.00	5.99
4		0.1	36.11	5.94
5	200	0.0001	35.54	5.89
6		0.001	35.35	5.97
7		0.01	39.12	5.90
8		0.1	38.16	5.70
9	300	0.0001	39.50	5.96
10		0.001	37.41	5.93
11		0.01	38.71	5.85
12		0.1	39.36	5.95
13	400	0.0001	37.61	5.94
14		0.001	38.41	5.90
15		0.01	38.33	5.91
16		0.1	35.82	5.99
17	500	0.0001	36.20	5.85
18		0.001	38.25	5.88
19		0.01	43.39	5.90
20		0.1	39.01	5.93

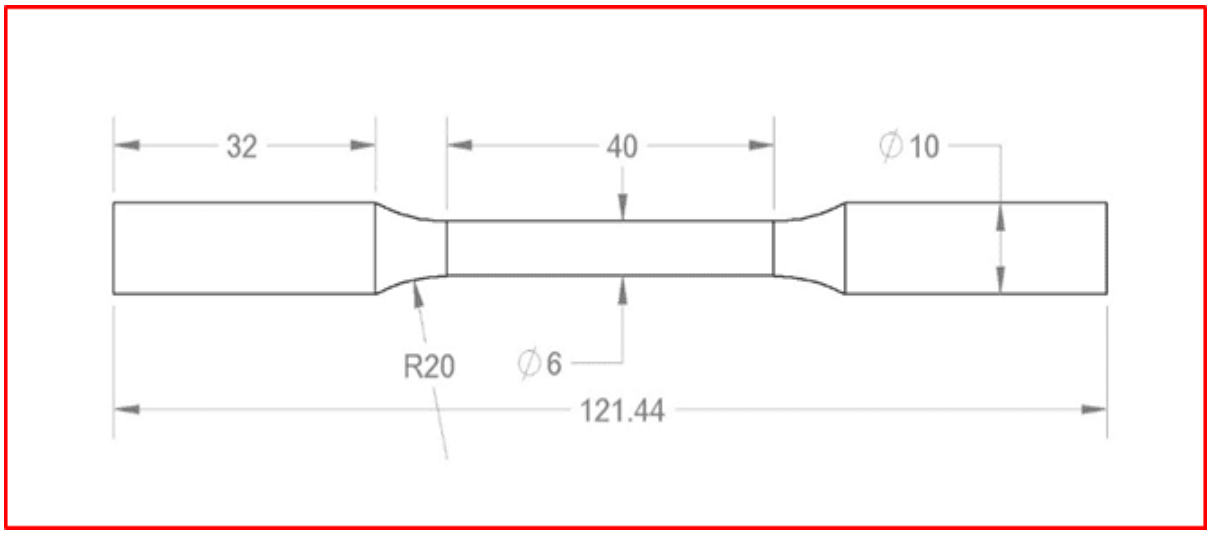

Fig. 2.6: Round tensile specimen

For validation of the proposed model, tensile tests are conducted on flat specimens with round notch. Fig. 2.7 shows the geometry and measurement definition of the round notch specimens. The tensile tests that are simulated and are being tabulated in the Table 2.3. These tests were also conducted in displacement control mode till fracture point.

Table 2.3: A summary of test matrix of flat specimen with round notch

Specimen no.	Test Temperature (°C)	Strain Rate (s^{-1})	Gauge length (mm)	Width (mm)	Thickness (mm)	Notch diameter (mm)
1	25°C	$0.0001s^{-1}$	31.59	5.94	5.96	0
2			30.81	5.96	3.93	0
3			31.12	5.93	1.99	0
4			32.21	9.98	5.96	3.90
5			31.58	10.00	3.90	3.90
6			29.59	9.98	2.00	3.96
7			34.57	13.98	3.92	8.00
8			34.92	13.99	1.96	7.98

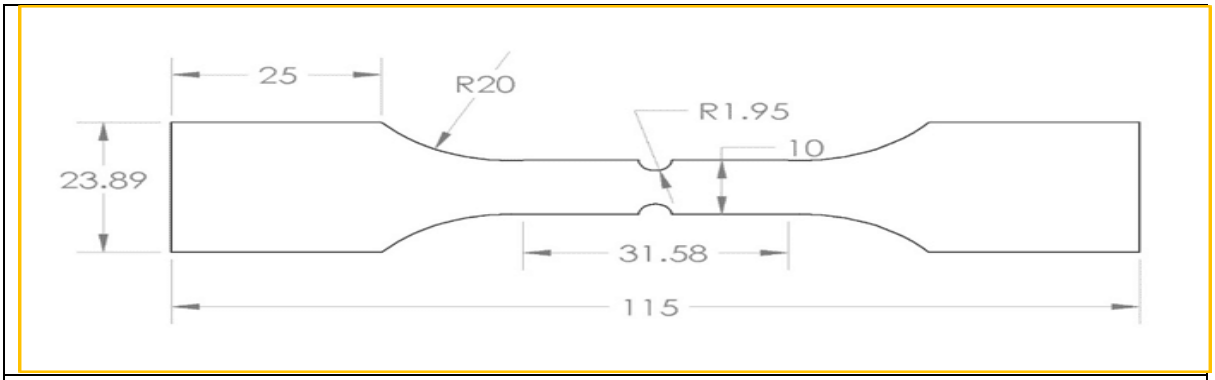

Fig. 2.7: Round notch flat specimen

2.2.2 Result from tensile experiments:

Fig 2.8 and Fig. 2.9 show the stress-strain curves from tensile tests at various strain rates and temperatures respectively. For every temperature and strain rate, the calculation of Young's modulus, yield strengths, and ultimate tensile strengths are done. To calculate Young's modulus, tensile stress- strain is plotted at the elastic or linear region. In the elastic region of the curve, the initial slope is declared as the Young's modulus with proportional to temperature and strain rate condition. The slope is considered for strain range in between 0.0001 to 0.001. Yield point is selected here 0.2 percent of the offset line in strain axis that cuts the tensile stress strain plot. The stress value for the yield point is considered as the material's yield strength. The Ultimate strength in tensile stress-strain plot is considered as the maximum tensile stress in the test for every temperature and strain rate.

From the result through experiment, it is observed that the values of Young's modulus, yield and ultimate strength changes with respect to both strain rate and temperature along with small scatter that can be expected. Young's modulus is defined by the atom's binding force, when the temperature increases with increase in the momentum of the atoms. As the momentum increases, the cohesive force between the atoms decreases, hence Young's modulus reduces with rise in temperature. Young's modulus does not vary significantly with respect to strain

rate. For tensile experiments at different temperatures and strain rates, some basic properties of tensile like young's modulus, yield strength, ultimate strength is calculated and shown below in table 2.4.

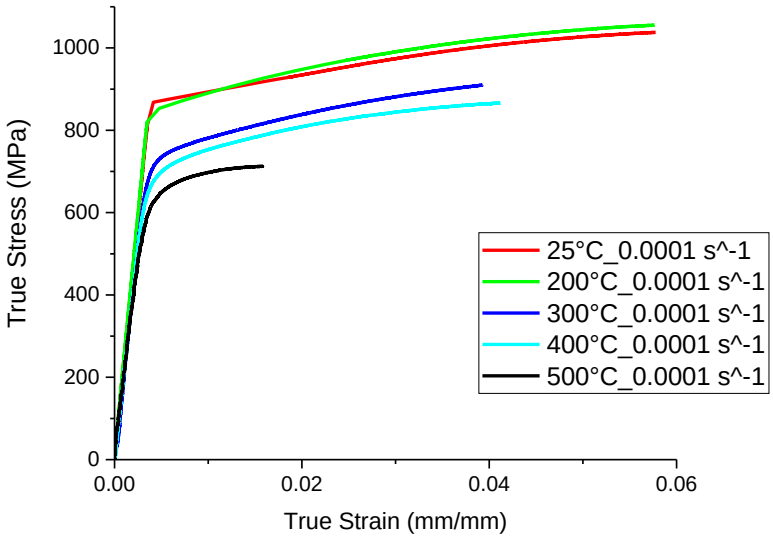

Fig. 2.8: Comparison of true stress vs. true strain curves with different temperatures at reference strain rate ($0.0001s^{-1}$).

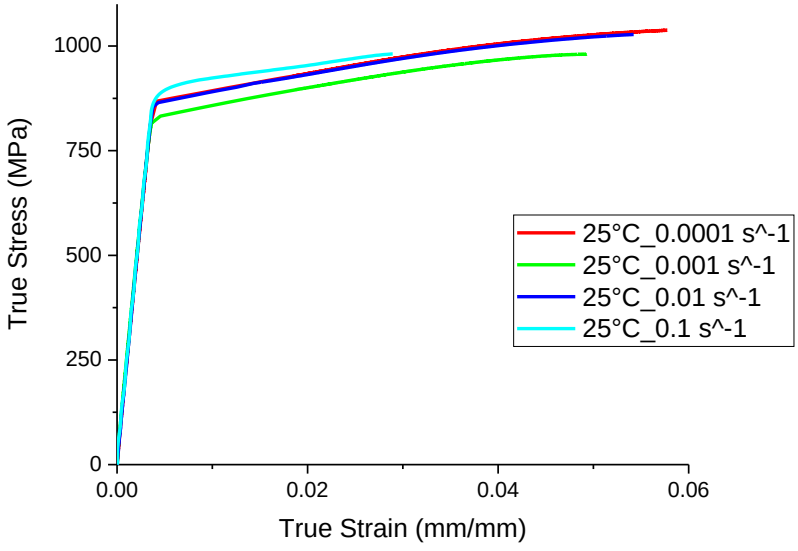

Fig. 2.9: Comparison of true stress vs. true strain curves with different strain rates at reference temperature (25°C)

Table 2.4: Variation of tensile properties with temperature and strain rate

Temperature (°C)	Mechanical properties	Strain Rate (s^{-1})			
		0.0001	0.001	0.01	0.1
25°C	Young modulus (GPa)	228.146	228.197	247.366	233.93
	yield strength (MPa)	883.13	847.12	886.453	898.569
	ultimate strength (MPa)	979.794	937.915	982.054	953.211
200°C	Young modulus (GPa)	233.380	194.632	200.937	227.938
	yield strength (MPa)	898.29	792.88	816.20	922.77
	ultimate strength (MPa)	996.517	883.31	895.832	962.105
300°C	Young modulus (GPa)	212.101	227.233	208.802	223.187
	yield strength (MPa)	739.00	738.909	748.90	740.78
	ultimate strength (MPa)	887.260	867.118	884.902	845.525
400°C	Young modulus (GPa)	201.480	206.243	219.705	213.776
	yield strength (MPa)	705.36	758.06	735.44	691.39
	ultimate strength (MPa)	831.042	914.599	903.819	810.515
500°C	Young modulus (GPa)	181.087	195.332	225.441	202.511
	yield strength (MPa)	652.66	693.38	698.11	669.18
	ultimate strength (MPa)	701.404	762.151	748.516	774.172

The variation of Young's modulus (E) with respect to strain rate and temperature are demonstrated in Figs. 2.10 and 2.11 respectively. Figs. 2.12 and 2.13 exhibits the variation of yield strength (σ_y) with respect to strain rate and temperature respectively. The variation of ultimate tensile strength (σ_{ut}) with respect to strain rate and temperature respectively are shown in Figs. 2.14 and 2.15.

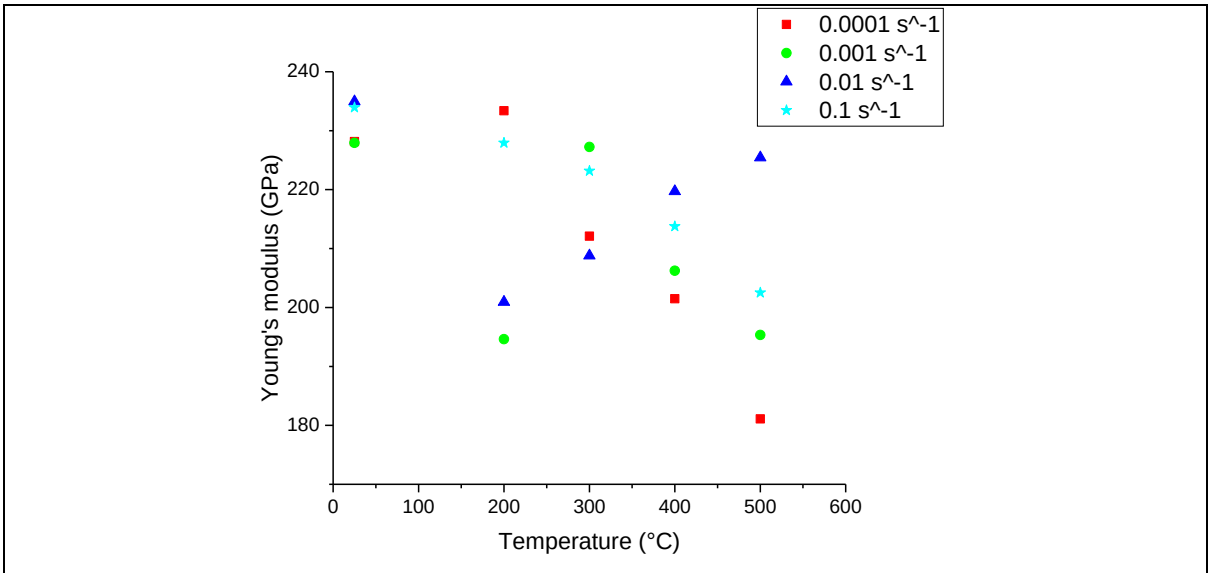

Fig. 2.10: Young's modulus at different temperature

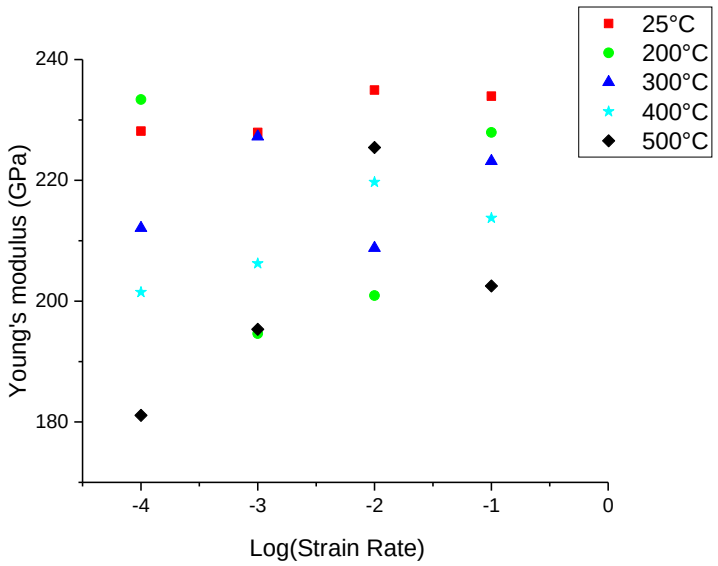

Fig. 2.11: Young's modulus at different strain rate

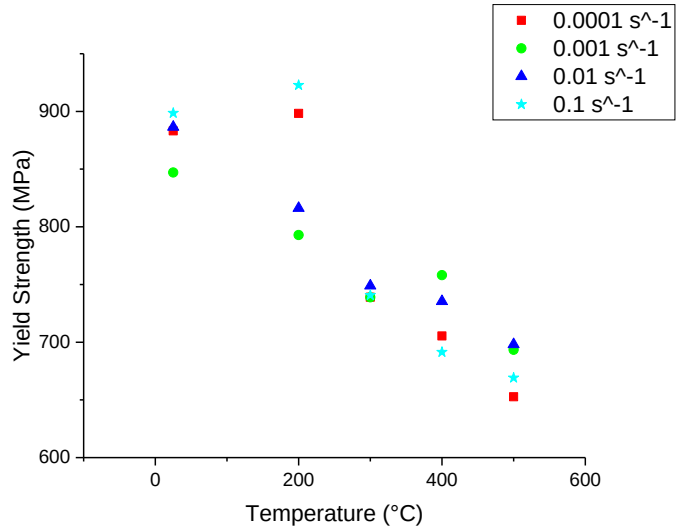

Fig. 2.12: Yield strength at different temperature

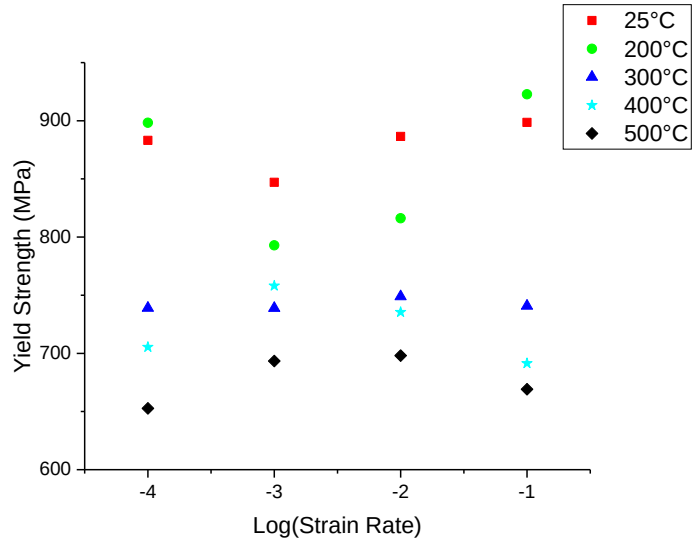

Fig. 2.13: Yield strength at different strain rate

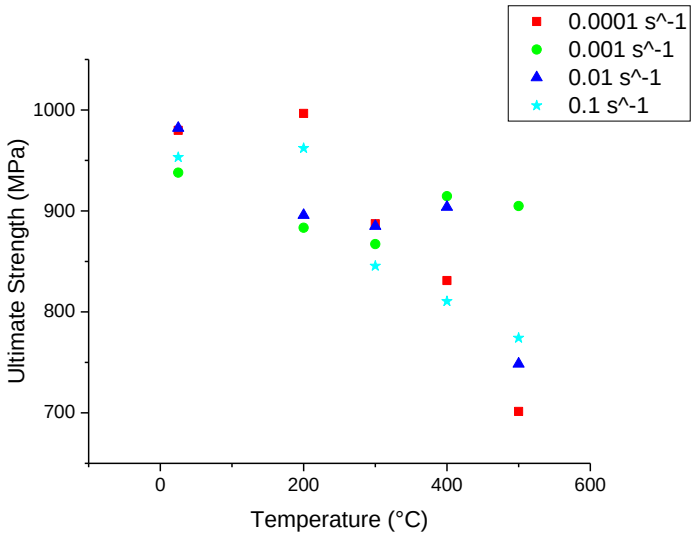

Fig. 2.14: Ultimate strength at different temperature

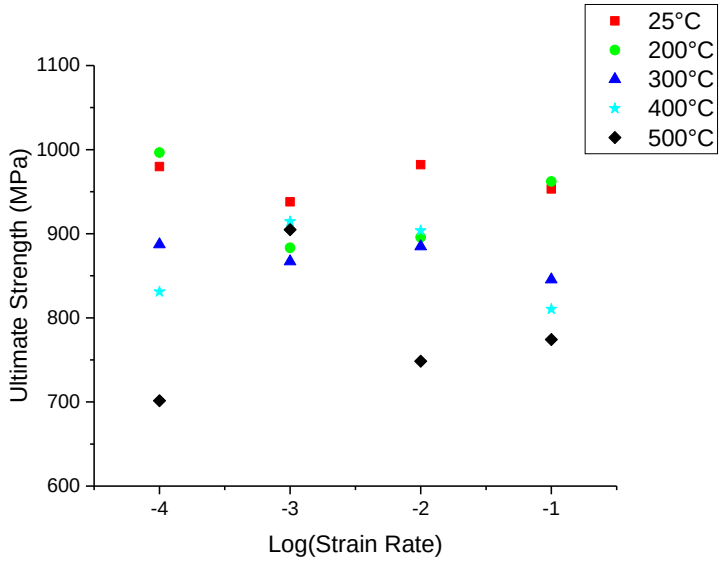

Fig. 2.15: Ultimate strength at different strain rate

From the experimental results, it is observed that the values of young's modulus, yield and ultimate strength changes with respect to both strain rate and temperature with the expectation of small scattering. In micro mechanical aspect, the strength of the material can be expressed by the rate of storage of dislocations in the regime of plastic. At the time of deformation of plastic, the diffusion of interstitial atoms shows restriction for the free glide of dislocation. Hence, the occurrence of strain hardening happens.

With rise in temperature, the momentum of the temperature increases that results in lowering strength. Strain rate has also shown influence for the strength of material. At the point of plastic deformation, the generation of some new dislocations occurs. With increase in strain rate, the rate of generation of new dislocation increases that results in increase of the dislocation density. Therefore, with increase in strain rate the strength of the material increases proportionally.

However, it is observed that at strain rates of $0.0001s^{-1}$, $0.001s^{-1}$ and $0.1s^{-1}$, there is a decrease in the values of young's modulus if the testing temperature is increased of the armour

steel specimen. But in strain rate of $0.01s^{-1}$, the value of young's modulus increases with increase in the testing temperature of armour steel. It can be perfectly observed that there is no uniformity between the variations of young's modulus with strain at all temperatures.

Now, it is observed that the values of both yield strength and that of ultimate strength for different temperatures will be depressed for all strain rates. However, for the increase value of yield strength if the strain rates increase, the change of ultimate strength value will not be much significant if strain rates increase for a particular temperature.

2.2.3 Flow properties of tensile experiment:

For the development of visco-plastic material model, the analysis on nature of flow curves for the tensile tests is very important. From the nature of the flow curve, the estimation of hardening function of true stress vs. plastic strain can be determined. In Figs. 2.8 and 2.9 a comparison between true stress vs. true strain curves are shown for different strain rates and temperatures respectively. Comparison curves are shown at minimum temperature/reference temperature (25°C) and at reference strain rate ($0.0001s^{-1}$) respectively.

From the above figs. 2.8 and 2.9, it can be clearly observed that this material is highly sensitive to strain rate and temperature. Now, the study of flow curves at higher temperature zone is done which aims to develop a visco-plastic model that is applicable for zones of high temperatures. To study the nature of flow curve, the variation of flow stress between increase of temperature and increase of strain rate at 0.5%, 2% and 4% plastic strain are plotted in Figs. 2.16 to 2.21.

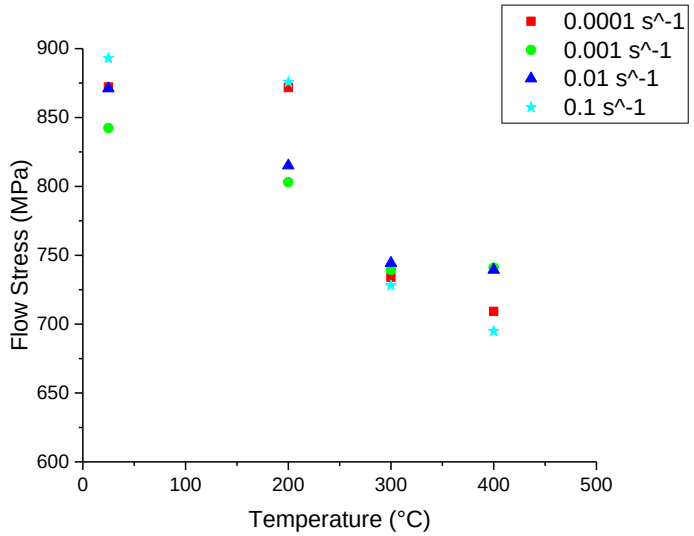

Fig. 2.16: Flow stress vs. temperature curve at different strain rate for 0.5% plastic strain

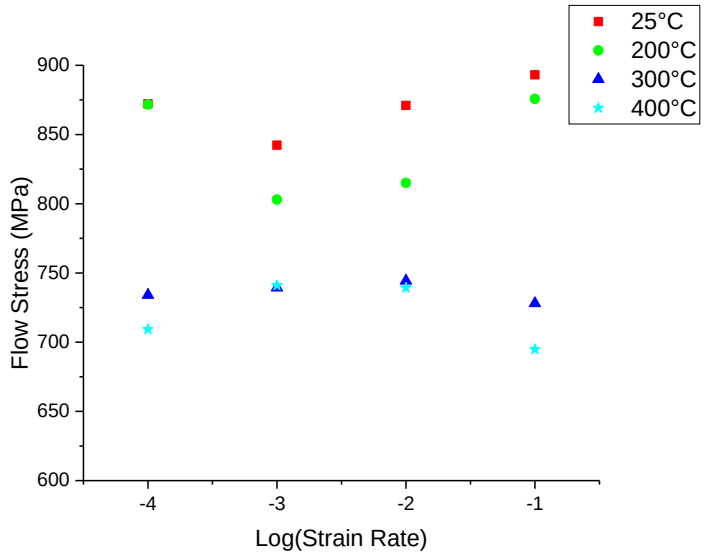

Fig. 2.17: Flow stress vs. strain rate curve at different temperature for 0.5% plastic strain

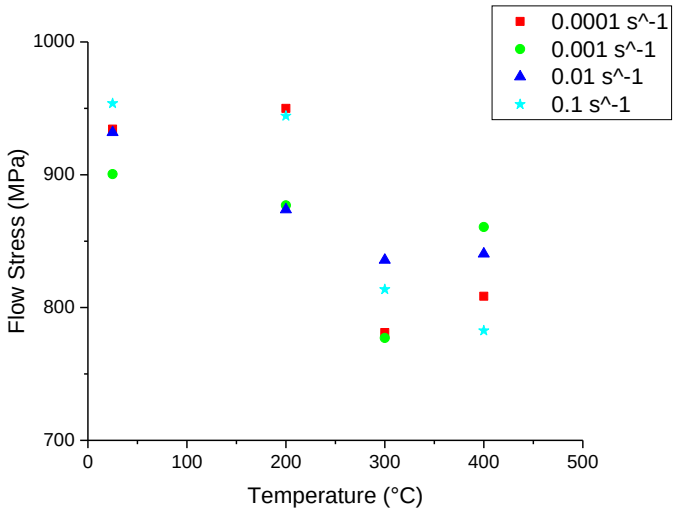

Fig. 2.18: Flow stress vs. temperature curve at different strain rate for 2% plastic strain

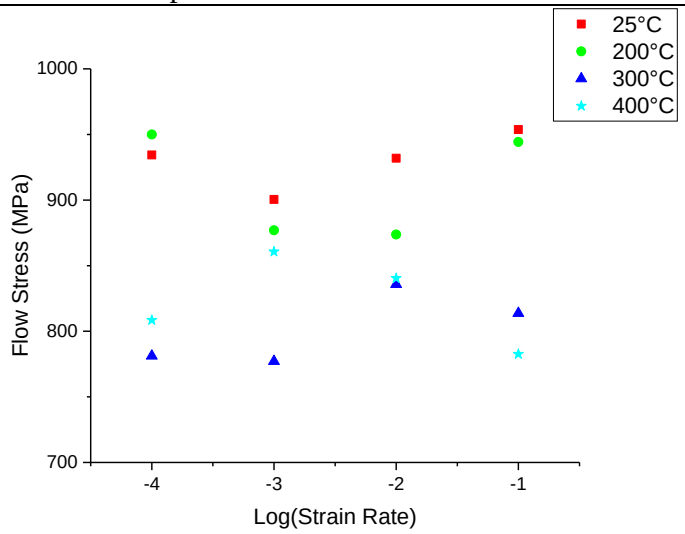

Fig. 2.19: Flow stress vs. strain rate curve at different temperature for 2% plastic strain

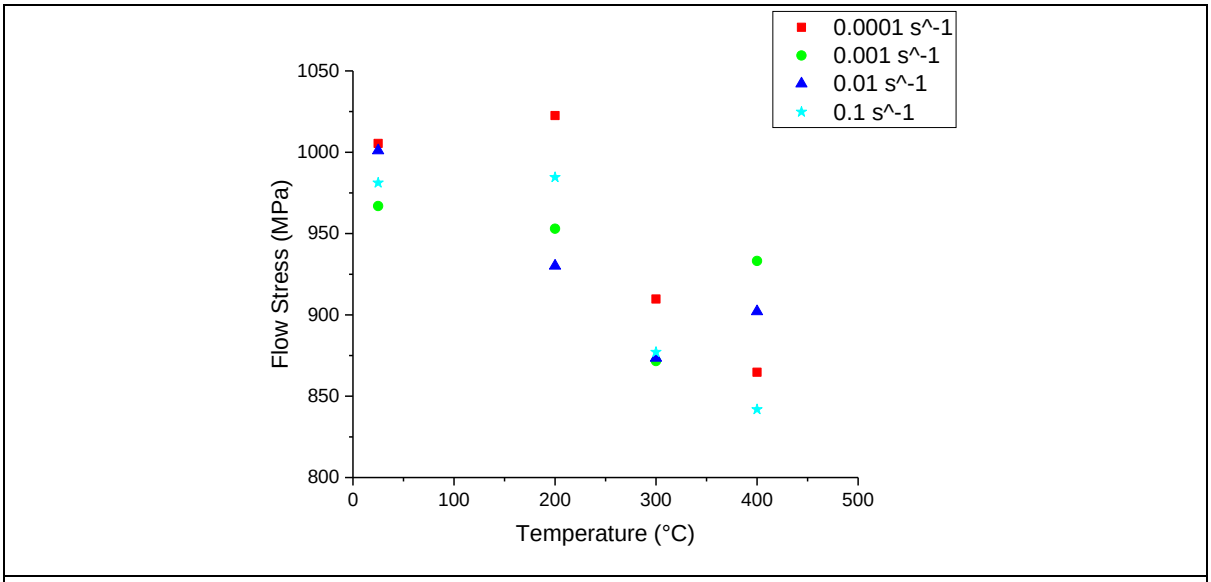

Fig. 2.20: Flow stress vs. temperature curve at different strain rate for 4% plastic strain

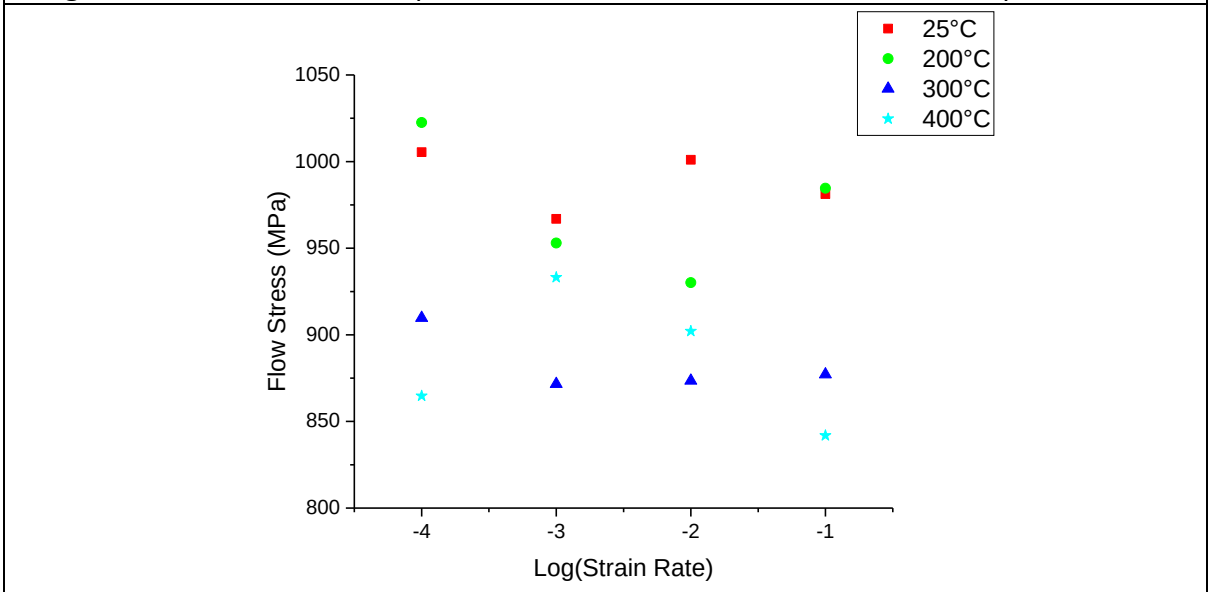

Fig. 2.21: Flow stress vs. strain rate curve at different temperature for 4% plastic strain

Here at 25°C, 200°C, 300°C and 400°C, the value of flow stresses decreases with increase in strain rate. Generally, flow stress increases with increase in strain rate that follows a power law expression, where the exponent is called strain rate sensitivity [68]. The exponent value is generally positive. But in this case, the sensitivity is showing negative, as decrease in stress, the strain rate increases. And the decrease in flow stress with increase in temperature is expected.

Chapter 3

3. Material model and finite element simulation:

3.1 Material model to capture temperature and strain rate effect on tensile properties:

Generally, there are two types of approach, to develop a constitutive model of phenomenological Visco-plastic, available in the literature surveys. One approach is considering, flow stress (σ_f) as function of plastic strain (ε_p), strain rate ($\dot{\varepsilon}$) and temperature (T) and another is considering rate of strain hardening ($d\sigma_f/d\varepsilon_p$) as function of plastic strain (ϵ_p), strain rate ($\dot{\varepsilon}$) and temperature (T).

In this study, the development of constitutive plasticity model is based on flow stress $\sigma_f(\varepsilon_p) = f(\varepsilon_p, \dot{\varepsilon}, T)$. Lin and Wagnor (LW) [74] proposed a constitutive model to capture temperature and strain rate effects for interstitial-free steel. The equation can be written as:

$$\sigma = A\left[1 - B\exp\left(C + D(T - T_0)\right)\varepsilon_P\right]\left(\frac{\dot{\varepsilon}}{\dot{\varepsilon}_0}\right)^m \left(\frac{T}{T_0}\right)^\beta \quad (3.1)$$

Where, A, B, C, D, m and b are material constants. The material constants are determined by curve fitting on stress-strain curve. But in this work, true stress and plastic strain are fitted with exponential curve as:

$$\sigma_f = A + B * \left(\varepsilon_p\right)^n \quad (3.2)$$

Where A, B, n are the material parameters which depends on temperature and strain rate. For each combination of strain rate and temperature, the values of A, B and n can be extracted from the fitted curve at every corresponding strain rate and temperature. Yield stress are related to A, and hardening is related to B and n. Thus, the variation of A, B and n is plotted with the temperature and strain rate separately.

Fig. 3.22 is the representation of fitting of true stress and plastic strain curve at particular temperature and strain rate. The values obtained for A, B and n at different temperature and strain rates are shown in Table 3.5 and Figs. 3.23 to 3.28 show the variation of A, B and n with respect to temperature and strain rate separately.

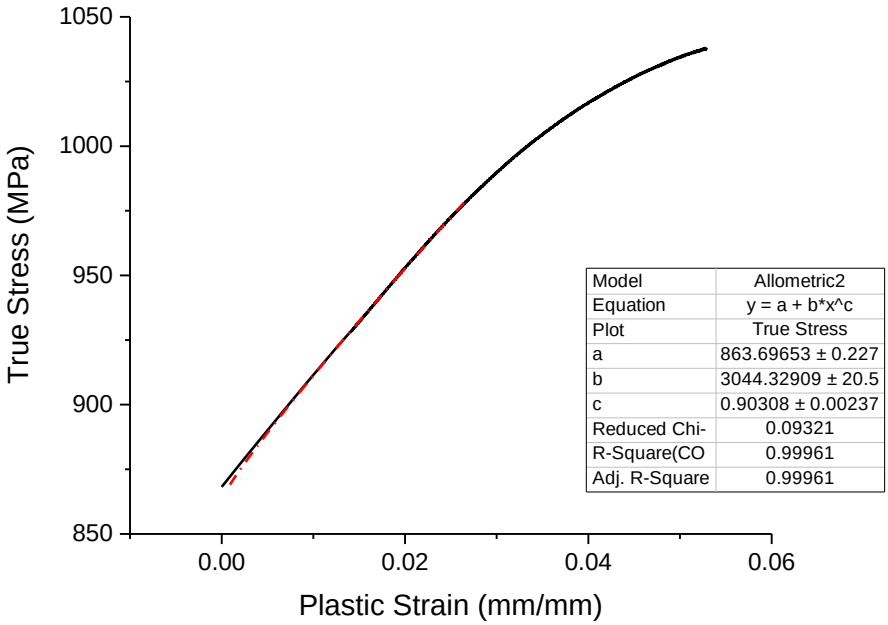

Fig. 3.22: Fitting curve with true stress versus plastic strain curve

Table 3.5: Values of fitting parameters at different temperatures and strain rates

Experimental fitting parameter		Temperature (°C)					
		25°C	200°C	300°C	400°C	500°C	
Strain Rate (s^{-1})	0.0001	862.81	799.21	742.14	701.912	645.075	A Value
	0.001	823.442	783.102	742.948	755.977	684.558	
	0.01	861.027	802.091	756.124	731.266	697.509	
	0.1	904.852	921.759	701.006	705.139	657.928	
	0.0001	3121.06	1223.46	2467.445	1444.27	626.444	B Value
	0.001	2385.351	2502.776	3048.352	1397.891	886.545	
	0.01	2805.52	2674.508	3127.504	1317.853	1440.937	
	0.1	1427.915	2181.527	1533.4407	2440.013	710.712	
	0.0001	0.90661	0.5073	0.76116	0.61117	0.45601	n Value
	0.001	0.83023	0.729	0.8367	0.60316	0.48129	
	0.01	0.8867	0.8743	0.86541	0.5863	0.6224	
	0.1	0.7949	0.9376	0.6291	0.81764	0.44012	

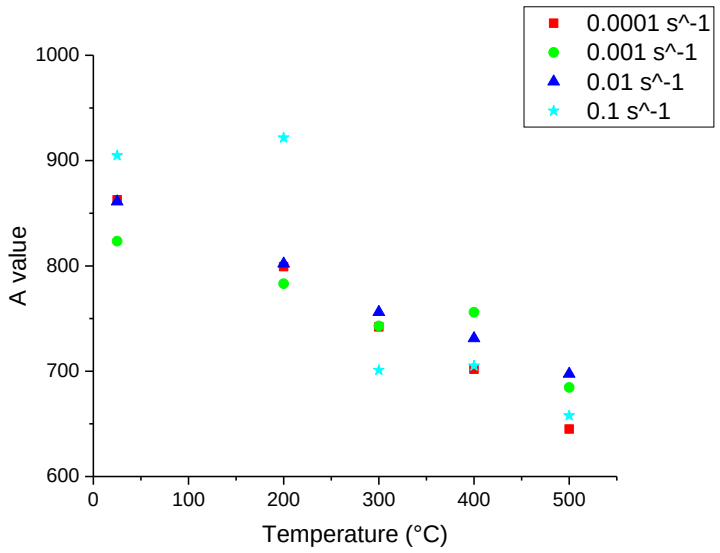

Fig. 3.23: Variation of A -value with temperature at different strain rates

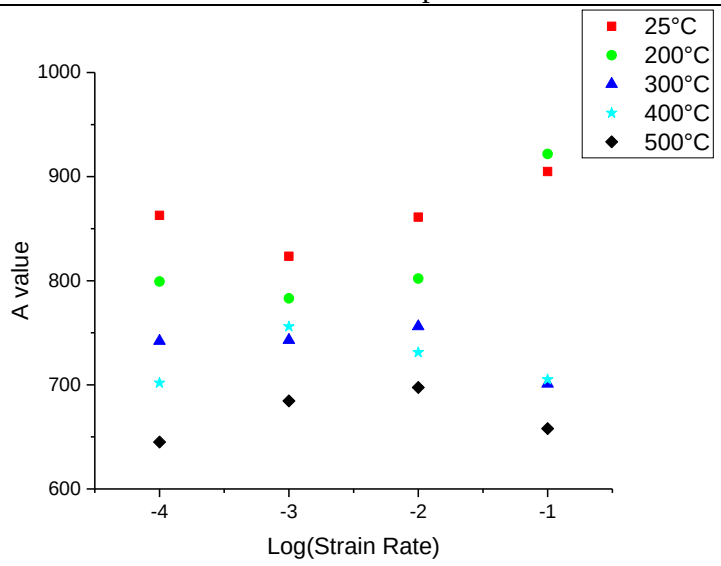

Fig. 3.24: Variation of A -value with strain rate at different temperatures

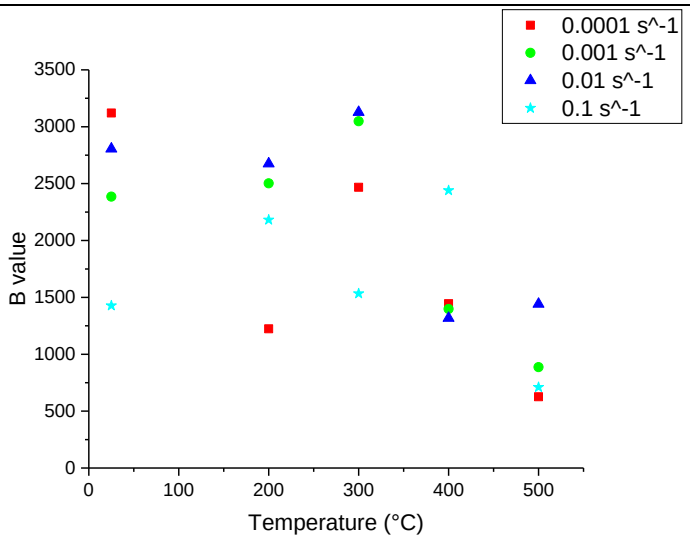

Fig. 3.25: Variation of B -value with temperature at different strain rates

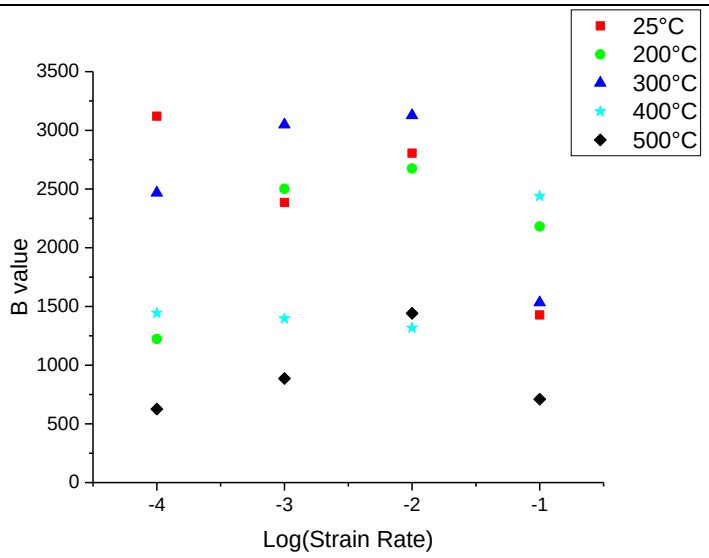

Fig. 3.26: Variation of B -value with strain rate at different temperatures

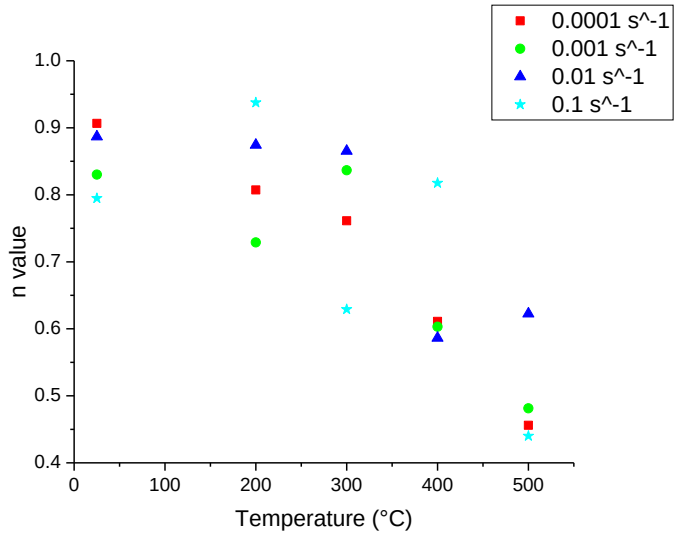

Fig. 3.27: Variation of n -value with temperature at different strain rates

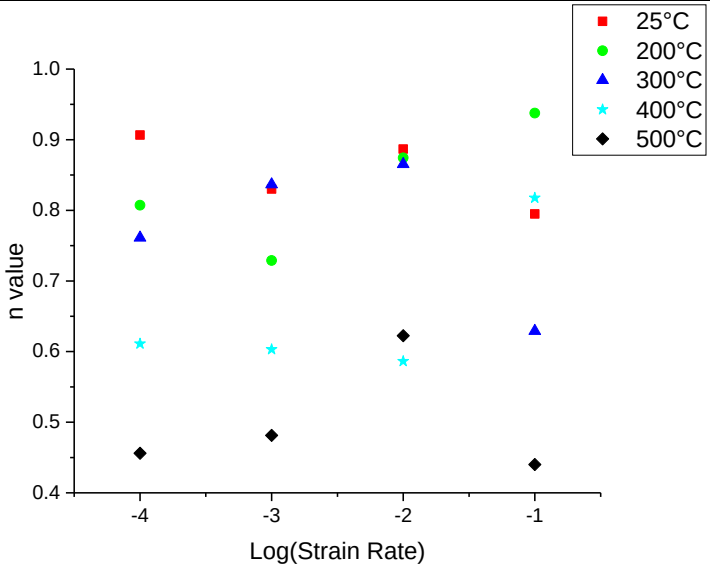

Fig. 3.28: Variation of n -value with strain rate at different temperatures

With temperature and strain rate, the variation of A exhibits a specific trend of decreasing with increase either in temperature at all the strain rates (Fig. 3.23) or in strain rate at all temperatures (Fig. 3.24). But in case of A vs. strain rate, the scatter observed is significantly much more. Similarly in Figs. 3.25 to 3.28, graph is plotted for the variations of B and n with temperature and strain rate. From those trends and scatter are prominently observed. From the experimental results, it can be observed that each of A, B and n is a function of both temperature and strain rate. In this work an attempt has been done to identify the functional form that is related to each of A, B and n with both temperature and strain rate and also the coefficient value of the equations using average method.

To obtain non-dimensional ratio of strain rate ($\dot{\varepsilon}^*$) and temperature (T^*), the testing temperatures and strain rates are respectively divided by a reference temperature (25°C) and a reference strain rate (0.0001 s^{-1}). To determine any particular trend from the above mentioned graph (figs.3.23 to 3.28), we are using average method for getting the points between the constants A_2, B_2 and n_2 with temperature keeping strain rate as a constant factor. Similarly, we are using average method for determining points between the constants A_1, B_1 and n_1 with strain rate keeping temperature as a constant factor.

Now, by applying different trial and error methods, we observe that the obtained values of the three material constants i.e. A, B and n with the non-dimensional form of temperatures and with logarithmic strain rates shows linearity in nature. The reason behind accepting the linear nature of the curve obtained falls with the observed number of the Pearson's value ('r') which is near about 0.96. So, from this it can be stated that each of A, B and n is a function of strain rate ratio ($\dot{\varepsilon}^*$) and temperature ratio (T*) individually. Figs. 3.29 to 3.34 mentioned below demonstrates the average values as well as the linearly fitted curves of A, B and n with the non-dimensional form of the temperature as well as the logarithmic strain rate.

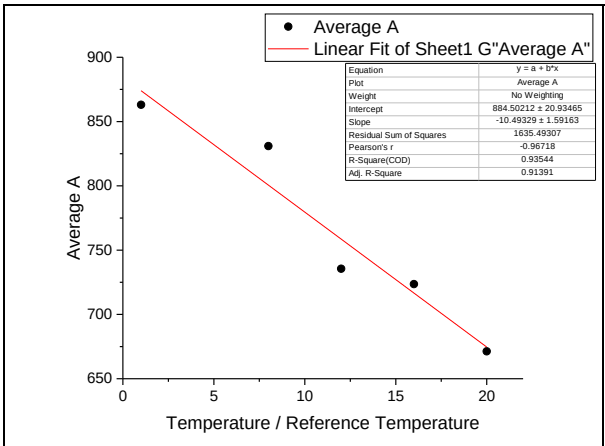

Fig.3.29: Linear fitted curve of average A-value with strain rate at different temperatures

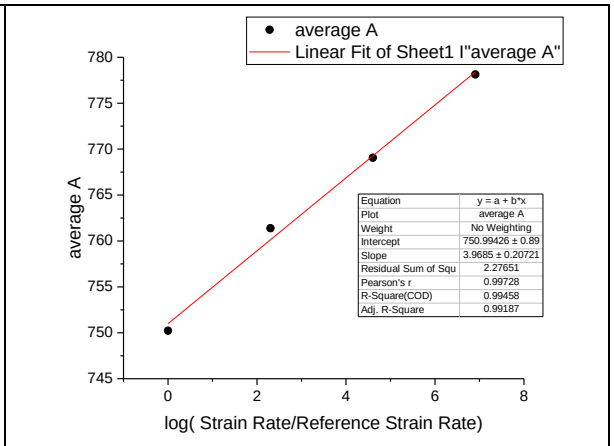

Fig.3.30: Linear fitted curve of average A-value with temperature at different strain rates

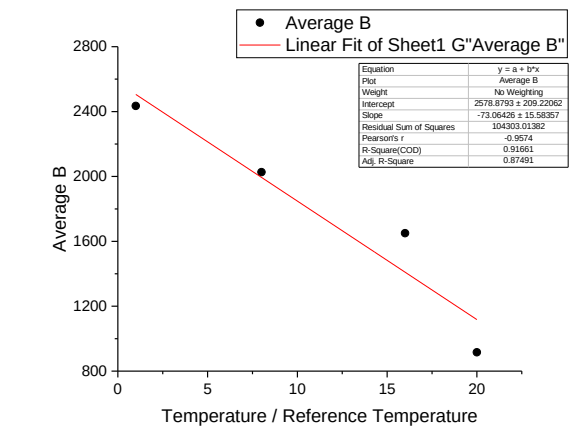

Fig.3.31: Linear fitted curve of average B-value with strain rate at different temperatures

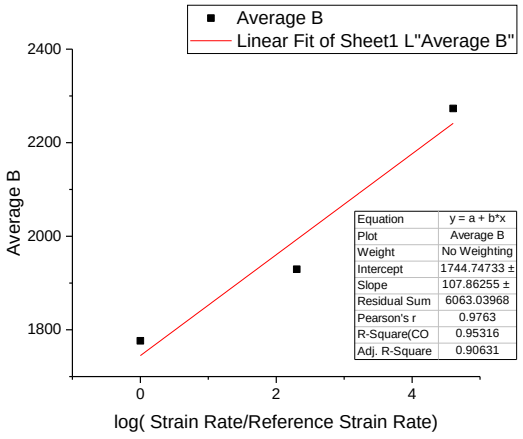

Fig.3.32: Linear fitted curve of average B-value with temperature at different strain rates

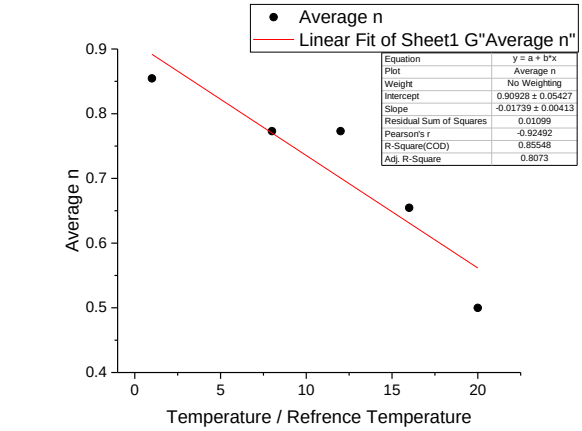

Fig.3.33: Linear fitted curve of average n-value with strain rate at different temperatures

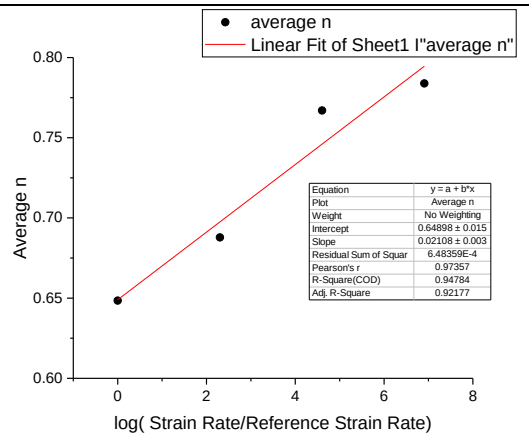

Fig.3.34: Linear fitted curve of average n-value with temperature at different strain rates

Now the functional form of A, B and n that obtained locally at different strain rate by taking temperature as constant is as follows:

$$A_1 = \{750.994 + 3.968 * \ln(\dot{\varepsilon}^*\} , \quad (3.3)$$

$$B_1 = \{1744.74 + 107.86 * \ln(\dot{\varepsilon}^*)\} , \quad (3.4)$$

$$n_1 = \{0.65 + 0.021 * \ln(\dot{\varepsilon}^*)\} \quad (3.5)$$

Also, the functional form of A, B and n obtained locally at different temperature when strain rate is considered as constant are as follows:

$$A_2 = \{884.50 - 10.49 * (T^*)\} \quad (3.6)$$

$$B_2 = \{2578.88 - 73.06 * (T^*)\} \quad (3.7)$$

$$n_2 = \{0.91 - 0.017 * (T^*)\} \quad (3.8)$$

Lastly, the global form of equation for each of A, B and n obtained by merging all the previous set of local equations of A_1, B_1, n_1, A_2, B_2 and n_2. To obtain the global equations we are using

geometric mean instead of arithmetic mean. The reason behind the usage of the method is the suitability for calculation of the mean values which provides more accuracy and rigidity. Arithmetic mean is basically used to calculate the average of the independent variables by nature and for the data sets that are not varying extremely. But, the variables in geometric mean possesses dependence and are widely skewed which is the basis of the proposed modelling where the constants are dependent on the temperatures and the strain rates. Also, one of the advantages is the unaffected fluctuations of sampling that is provided by geometric mean method. Therefore, in this context, geometric mean is perfectly suitable in this proposed modelling. The global equations are as follows:

$$A = [A_1 * A_2]^{0.5} = [\,\{750.99 + 3.96 * \ln(\dot{\varepsilon}^*)\} * \{884.50 - 10.49 * (T^*)\}\,]^{0.5} \quad (3.9)$$

$$B = [B_1 * B_2]^{0.5} = [\,\{1744.74 + 107.86 * \ln(\dot{\varepsilon}^*)\} * \{2578.88 - 73.06 * (T^*)\}\,]^{0.5} \quad (3.10)$$

$$n = [n_1 * n_2]^{0.5} = [\,\{0.65 + 0.021 * \ln(\dot{\varepsilon}^*)\} * \{0.91 - 0.017 * (T^*)\}\,]^{0.5} \quad (3.11)$$

$$\sigma_f = A + B * (\varepsilon_P)^n \quad (3.12)$$

The above mentioned equations is the final analytical form of the proposed model.

Now, for the validation of the analytical equations, we will calculate the values of the material constants i.e., A, B and n obtained from the above set of analytical equations for every condition of temperatures and strain rates. From the equation 3.12, we will determine the values of flow stress from the range between initial and ultimate value arbitrarily of plastic strain leaving certain intervals. To find out the true stress we have to take into consideration the whole region but by calculating separately. The first part is to determine the true stress in the elastic region i.e., till the yield point by using the generalized Hooke's Law which is as follows:

$\sigma_f = E(\dot{\varepsilon}, T) * \varepsilon_e$, when $\sigma < A_1$ or yield strength (3.13)

And the second part is to calculate the true stress or the flow stress in the plastic region by the equation 3.12 above mentioned. Now, by merging both the equations 3.12 and 3.13, we will compare the analytical data points with the experimental flow curve for validation. From figs. 3.35 to 3.39, we can observe that there is a good coordination between the analytical data points and the experimental curves.

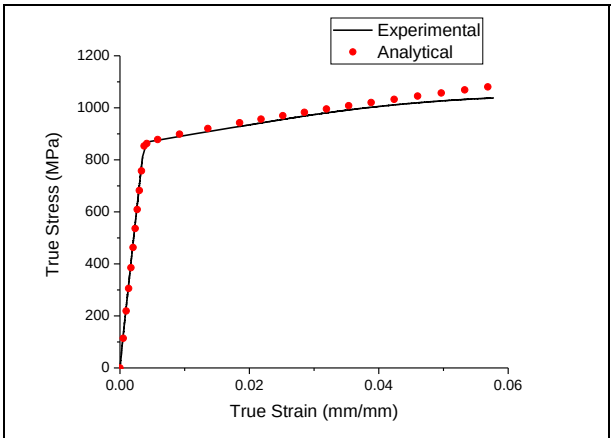

Figs.3.35: Comparison between experimental curve and analytical data points at 25°C temperature and 0.0001 s^{-1} strain rate.

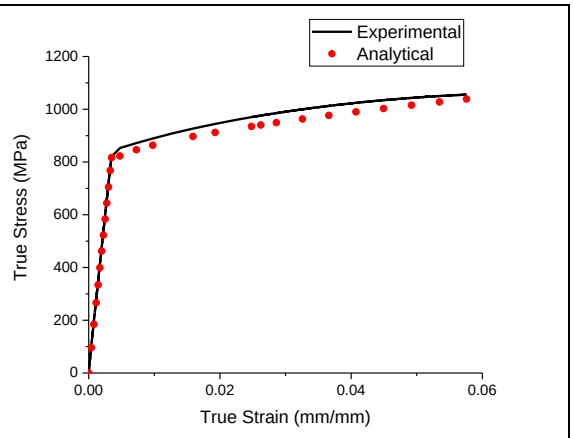

Figs.3.36: Comparison between experimental curve and analytical data points at 200°C temperature and 0.0001 s^{-1} strain rate.

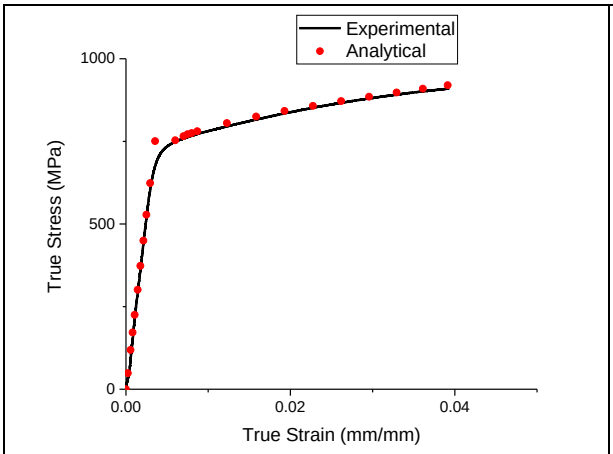

Figs.3.37: Comparison between experimental curve and analytical data points at 300°C temperature and 0.0001 s^{-1} strain rate.

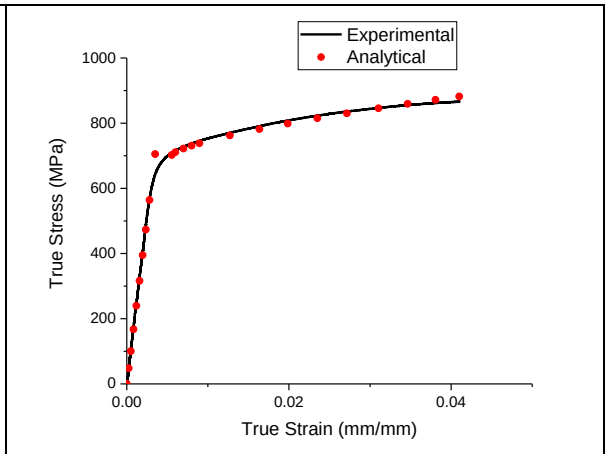

Figs.3.38: Comparison between experimental curve and analytical data points at 400°C temperature and 0.0001 s^{-1} strain rate.

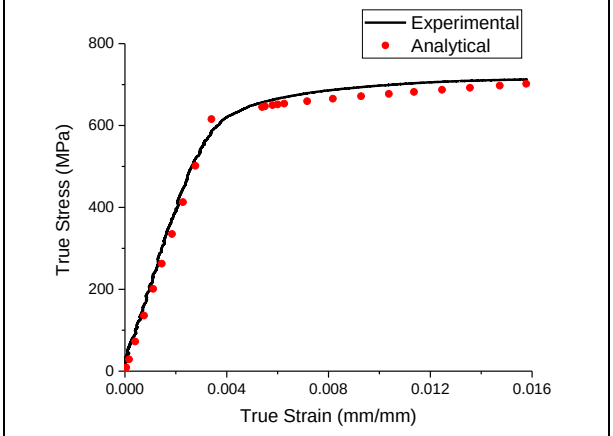

Figs.3.39: Comparison between experimental curve and analytical data points at 500°C temperature and 0.0001 s^{-1} strain rate.

3.2 Finite Element analysis of tensile experiment:

In this proposed modelling Abaqus standard is used as medium of Finite Element Analysis. The implementation used here is user defined material model or UMAT sub-routine. As because in Abaqus commercial package library, this type of material model sub-routine is unavailable. For this very fact, we made our own user defined material model (UMAT) sub-routine for our proposed model.

In this work, the correlation of A, B and n with temperature and strain rate is obtained by simulation for any tensile test in any temperature at elevated region and strain rate is directly employed by this material model considering all its optimum material properties. To validate, the suggested constitutive model and material properties along with the experimental result. Finite Element (FE) analysis of tensile tests for different temperature and strain rates are simulated using Abaqus 6.8 FE package. FE method is widely used for analysing the elastic-plastic response of structure.

For Abaqus 6.8 commercial package, to solve a Finite Element problem, three procedures are considered. That is:

(I) Pre-processing
(II) Solution of FE analysis as defined in pre-processing
(III) Post processing

3.2.1 Pre-processing:

In this part, the Finite Element model is defined by its physical features as well as input parameters like (i) the structure of geometry, (ii) material properties that are employed, (iii) element type choice, (iv) discretization or meshing of the whole body, (v) application of boundary condition, (vi) desirable loading scheme, (vii) describe the time step etc.

To employ the material properties is an important procedure as the ability to withstand external force is much dependent on the material that has chosen. What actually causes a component to fail? The component will fail or gets permanently deformed if the load limit is exceeded. To analyse mechanical strength, the behaviour of the material in the presence of external forces, such as component reaction (e.g., deflection) is critical.

In the process of model preparation, the next step is the application of boundary conditions on it. The requirement of limitation is necessary to keep the component from moving through. Further boundary condition specifies the external forces of the components, as there will be no deflection to occur without them. There is an effect on component parts by loads such as pressure or force that have been defined by the user for given numerical values. This is the complete requirement to conclude a successful calculation.

Pre-processing, often described as model preparation which is actually the most time taking step of the FEA. This generally refers to no construction of components into small areas, the finite (small, but finite) elements, for the overview of the component surface. This process is known as Meshing. Terms like "free" and "mapped" meshes are used more often. Although mapped mesh provides incredibly regular meshes, these are especially convenient for simple geometries.

The method of free-meshing is mainly based for the triangular surfaces, for creation of tetrahedrons and for majority of curved geometries. For this study, the quarter axi-symmetric model is meshed using continuum 3D8 node brick element (C3D8R). The material properties is defined using a user defined material sub-routine (UMAT). For the sub-routine, the primary material laws are followed by the material model that has been developed. The boundary conditions and meshing are shown in the Figs. 3.40 and 3.41.

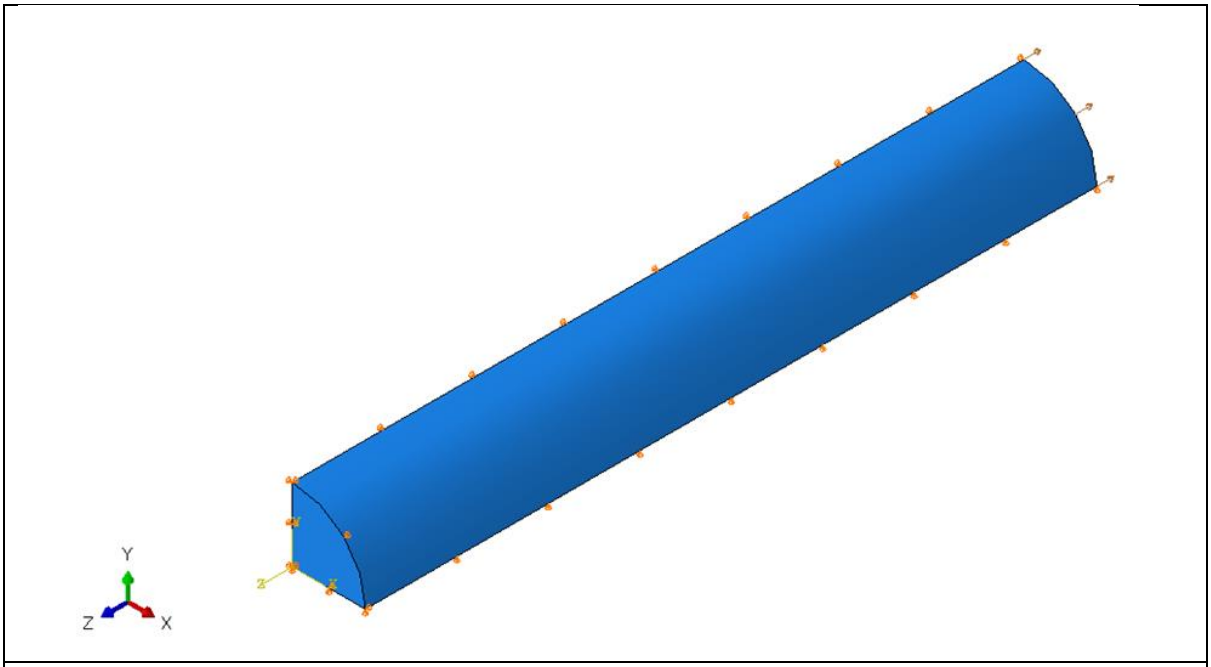

Fig. 3.40: Boundary conditions of quarter tensile specimen

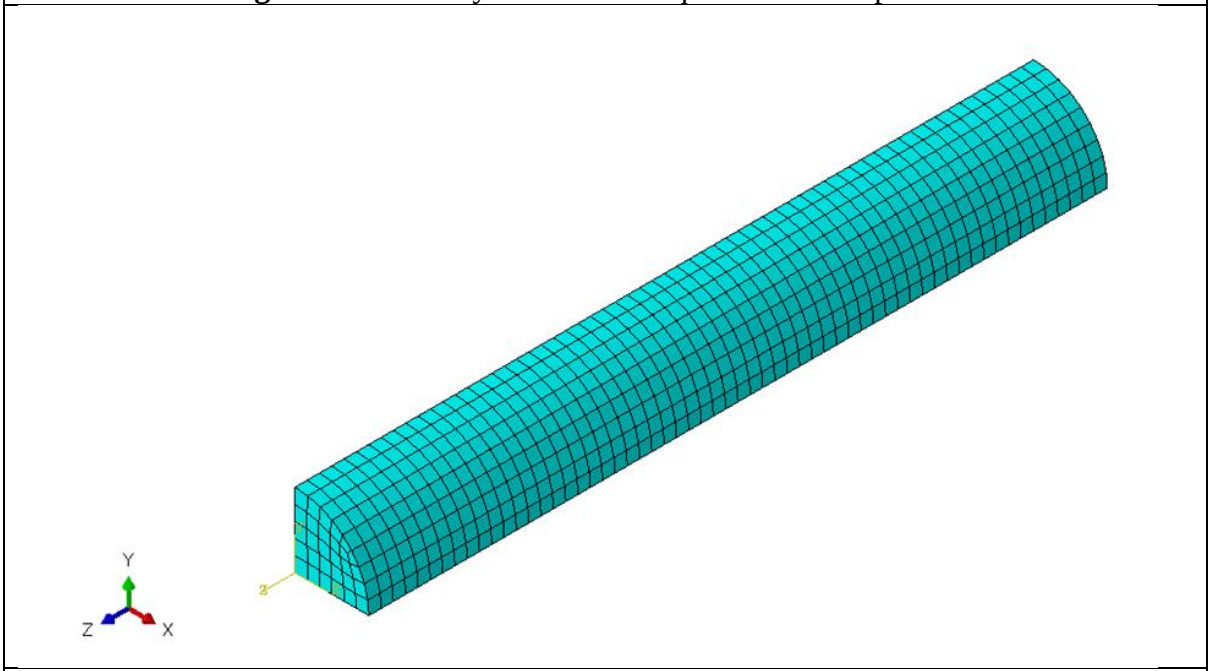

Fig. 3.41: Meshing of quarter tensile specimen

3.2.2 Solution of Finite Element (FE) analysis:

For the solution phase to analyse FE, the solver basically uses numerical method for solving the problem. In this study, the process to update stress is carried out by using an implicit methodology and to solve the differential equations the Backward Euler method is used. In Hooke's law, the tensor form is used for isotropic elastic behaviour. However, Von-Misses plasticity with isotropic hardening is used for plastic behaviour. Stress update is achieved using an implicit stress update (Backward Euler method) algorithm written as a sub-routine. A flow diagram is shown in Fig. 3.42 for better understanding of the algorithm. The Newton-Raphson method is used to make this prediction iteratively.

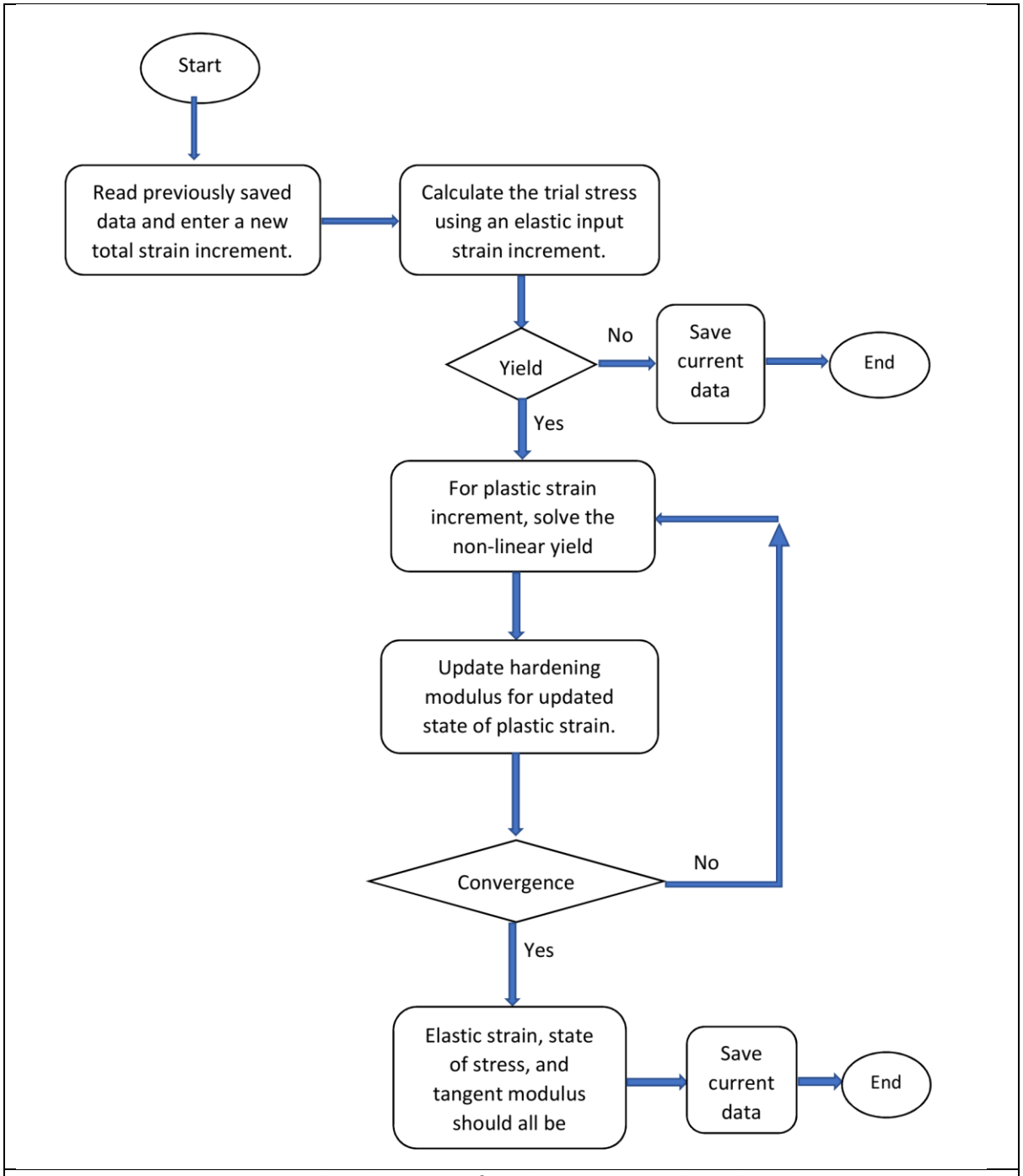

Fig. 3.42: Flow diagram of implicit stress update algorithm

3.2.3 Backward Euler integration scheme: the radial return method:

The Euler method is same as the Backward Euler method, except the nature is implicit. To converge the elastic predictor and the plastic corrector, one trial stress can be predicted. Initially, an increase of the total strain is given elastically to predict a trial stress, and then the trial stress converges onto the revised yield surface using a plastic corrector, which is a projection to the predicted trial stress. Because the phenomena of hardening are isotropic in nature, this method is termed as the radial return method. A schematic picture is shown in fig. 3.43.

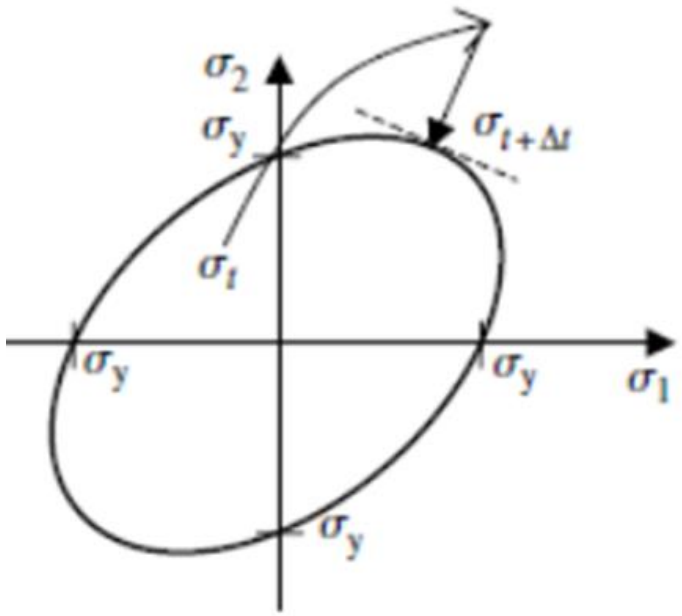

Fig. 3.43: Schematic representation of radial return method

In equation 3.14 current state of stress with previous state of stress, elastic predictor and plastic corrector is shown.

$$\sigma_{ij}^{1} = \sigma_{ij}^{0} + \mu\Delta\varepsilon_{ij} + \lambda Tr\left(\Delta\varepsilon_{ij}\right) - \mu\Delta\varepsilon_{ij}^{p} \tag{3.14}$$

Where σ_{ij}^{1} is current state of stress, and σ_{ij}^{0} is previous state of stress, μ and λ are Lame's constant, $\Delta\varepsilon_{ij}$ is the total strain increment in the time step, Tr ($\Delta\varepsilon_{ij}$) is equal to $\sum\Delta\varepsilon_{ij}$ which represents the volumetric strain increment.

Now current state of stress can be written in terms of equivalent plastic strain increment and flow vector in the following equation 3.15

$$\sigma_{ij}^{1} = \sigma_{ij}^{trial} - 2G\Delta\varepsilon_{eq}^{p}\frac{3}{2}\left(\frac{s_{ij}-\alpha_{ij}}{s_{mises}}\right) \tag{3.15}$$

Where trail stress (σ_{ij}^{trail}) $= \sigma_{ij}^{0} + \mu\Delta\varepsilon_{ij} + \lambda Tr(\Delta\varepsilon_{ij})$, G is the shear modulus, is equal to μ/2 the yield function, using trial stress can be written as:

$$f = s_{mises} - r - \sigma_y = s_{mises}^{trail} - 3G\Delta\varepsilon_{eq}^{p} - r - \sigma_y \tag{3.16}$$

For isotropic hardening condition $f(\sigma, \varepsilon^p) = 0$ or, $s_{mises} - r - \sigma_y = 0$ (3.17)

Where r is the linear hardening stress and σ_y is the primary yield stress

In the above equation it is seen that yield (f) can be a non-linear function of $\Delta\varepsilon_{eq}^{p}$. The non-linear equation can be solved using Newton's method

$$f + \frac{\delta f}{\delta\Delta\varepsilon_{eq}^{p}}d\Delta\varepsilon_{eq}^{p} + \cdots = 0 \tag{3.18}$$

For linear hardening $r = h\Delta\varepsilon_{eq}^{p}$ so that

Where, $\frac{\delta r}{\delta \Delta \varepsilon_{eq}^{p}} = h$ (3.19)

Now substituting equation 3.17, into equation 3.18 by using equation 3.19 gives

$$s_{mises}^{trail} - 3G\Delta\varepsilon_{eq}^{p} - r - \sigma_y + (-3g - h)d\Delta\varepsilon_{eq}^{p} = 0 \quad (3.20)$$

Rearranging the above equation 3.20 gives

$$d\Delta\varepsilon_{eq}^{p} = \frac{s_{mises}^{trail} - 3G\Delta\varepsilon_{eq}^{p} - r - \sigma_y}{3G+h} \quad (3.21)$$

In the iterative form equation 3.21 can be written as

$$d\Delta\varepsilon_{eq}^{p} = \frac{s_{mises}^{trail} - 3G\Delta\varepsilon_{eq}^{p^i} - r^i - \sigma_y}{3G+h} \quad (3.22)$$

$$\Delta\varepsilon_{eq}^{p^{i+1}} = \Delta\varepsilon_{eq}^{p^i} + d\Delta\varepsilon_{eq}^{p} \quad (3.23)$$

Where i is the iteration number.

3.2.4 Post Processing:

After the completion of the structural body or specimen's simulation, some responses regarding elasto-plastic are extracted in the form of output. For this study, the main elasto-plastic behaviour is the load response, the deformation at each node, stress and strain values of each element. In Fig. 3.44 Von-Misses stress distribution at 25°C and 0.001 s^{-1} strain rate is shown. The main aim of the Finite Element simulation is to compare between the simulated stress-strain curves and the experimental stress-strain curves. Also, to validate the material model. For the result and discussion section, simulated curves are shown along with respective experimental curves.

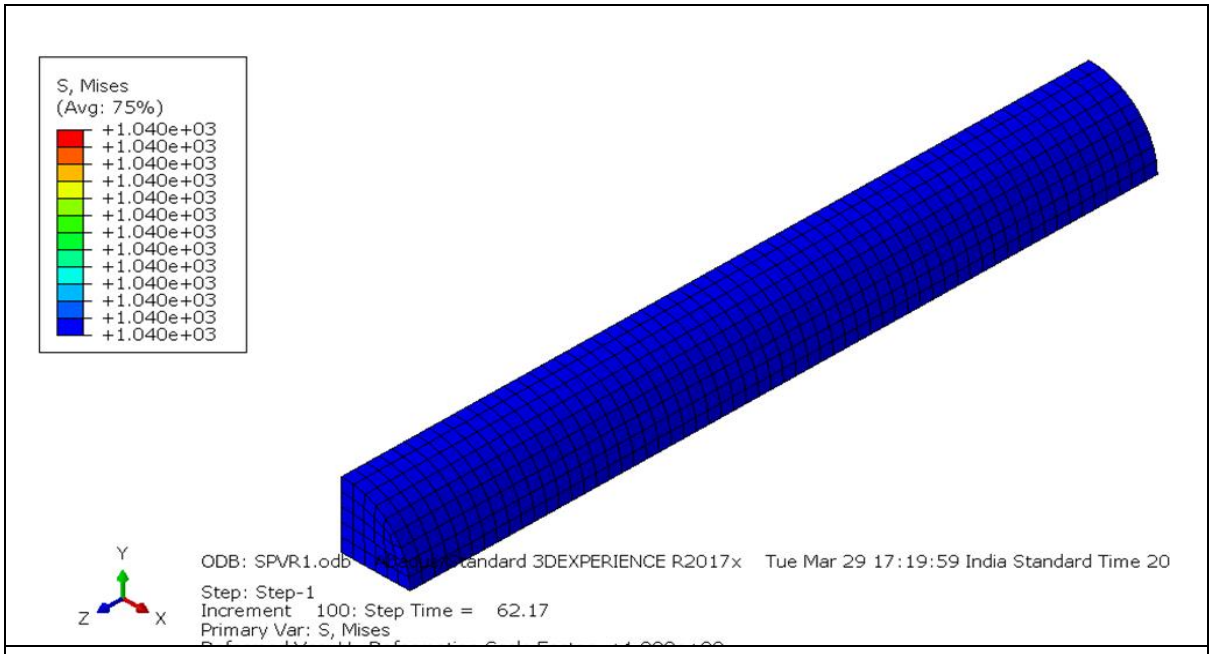

Fig. 3.44: Von-Mises stress distribution at 25°C and 0.001s^{-1} strain rate.

Chapter 4

4. Results and discussion of tensile simulation:

The results of experiment and simulation of the uniaxial tensile test over a wide range of temperatures (room temperature to 500 °C) and strain rates ($0.0001s^{-1}$ to $0.1s^{-1}$) are compared in the form of variation of the true stress exerted on the specimen with respect to true strain.

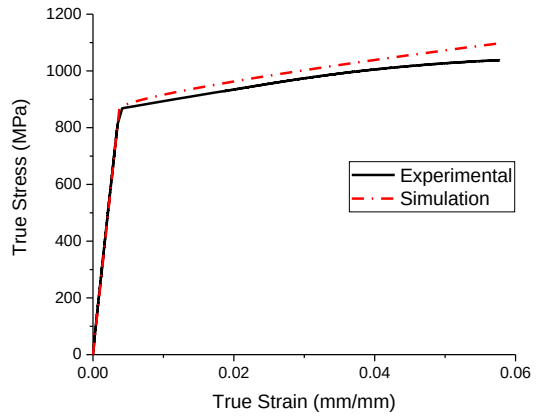

Fig. 4.45: Comparison of simulation and experimental true stress-true strain curves for 25°C at $0.0001s^{-1}$ strain rate.

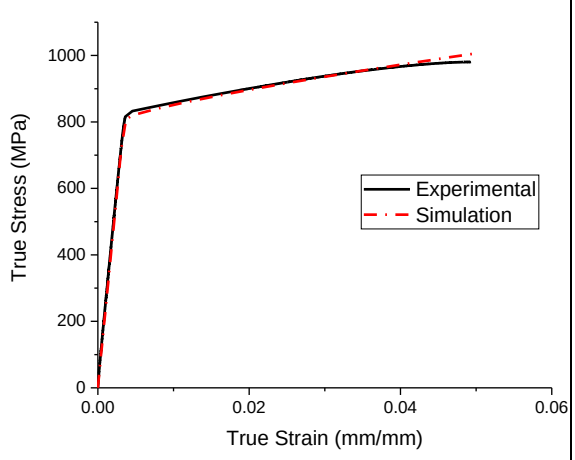

Fig. 4.46: Comparison of simulation and experimental true stress-true strain curves for 25°C at $0.001s^{-1}$ strain rate.

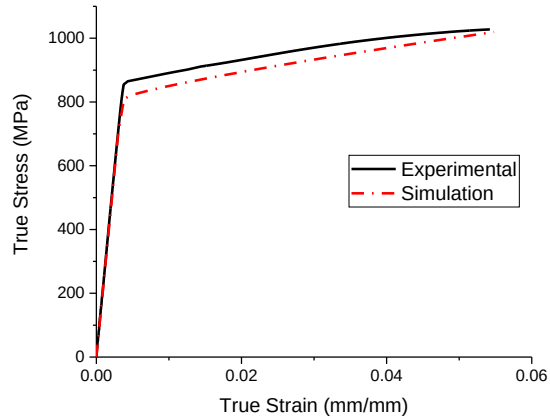

Fig. 4.47: Comparison of simulation and experimental true stress-true strain curves for 25°C at $0.01s^{-1}$ strain rate.

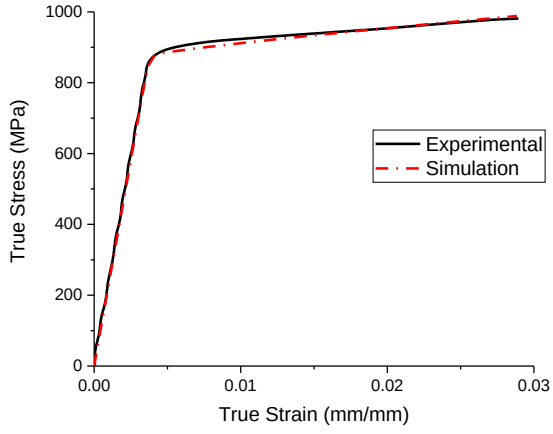

Fig. 4.48: Comparison of simulation and experimental true stress-true strain curves for 25°C at $0.1s^{-1}$ strain rate.

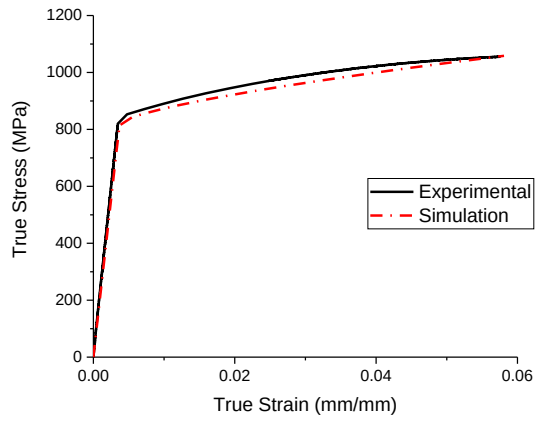

Fig. 4.49: Comparison of simulation and experimental true stress-true strain curves for 200°C at $0.0001s^{-1}$ strain rate.

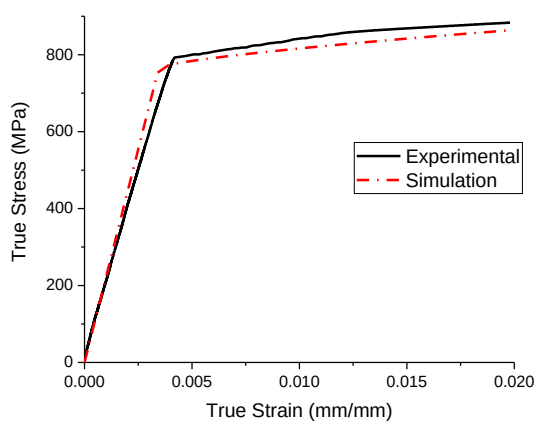

Fig. 4.50: Comparison of simulation and experimental true stress-true strain curves for 200°C at $0.001s^{-1}$ strain rate.

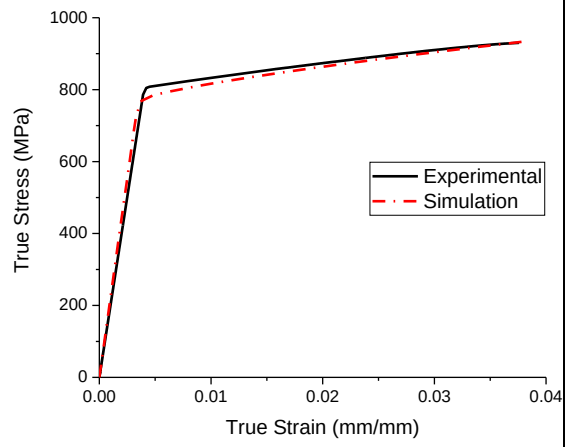

Fig.4.51: Comparison of simulation and experimental true stress-true strain curves for 200°C at $0.01s^{-1}$ strain rate.

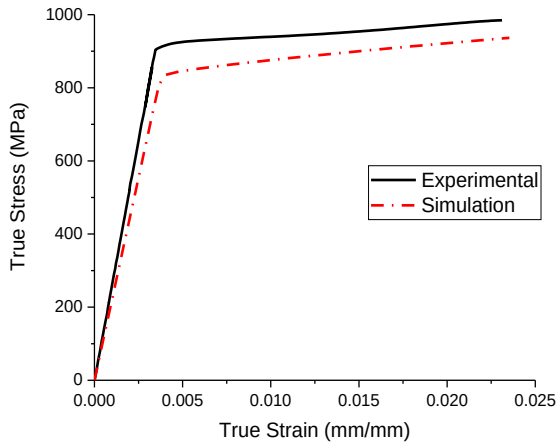

Fig. 4.52: Comparison of simulation and experimental true stress-true strain curves for 200°C at $0.1s^{-1}$ strain rate.

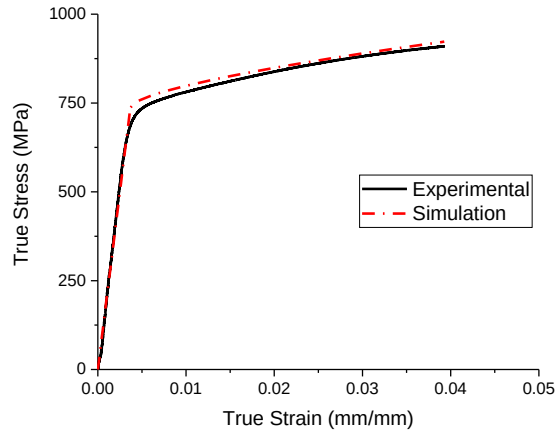

Fig. 4.53: Comparison of simulation and experimental true stress-true strain curves for 300°C at $0.0001s^{-1}$ strain rate.

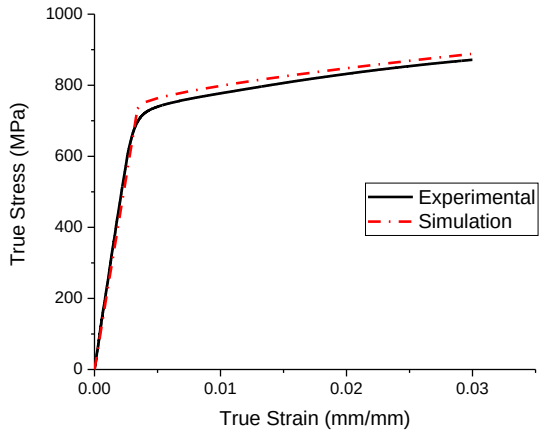

Fig. 4.54: Comparison of simulation and experimental true stress-true strain curves for 300°C at $0.001s^{-1}$ strain rate.

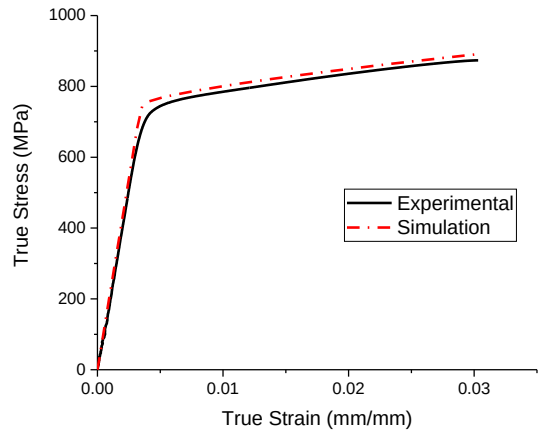

Fig. 4.55: Comparison of simulation and experimental true stress-true strain curves for 300°C at $0.01s^{-1}$ strain rate.

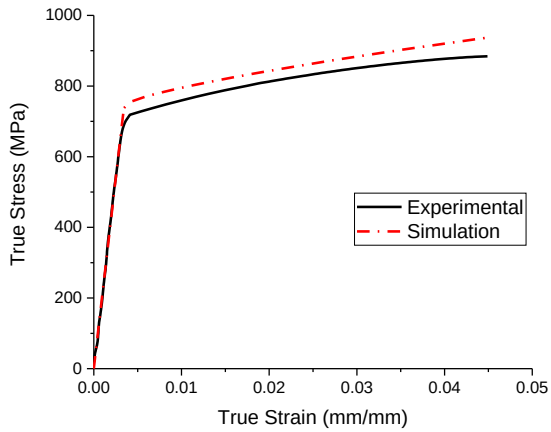

Fig. 4.56: Comparison of simulation and experimental true stress-true strain curves for 300°C at $0.1s^{-1}$ strain rate.

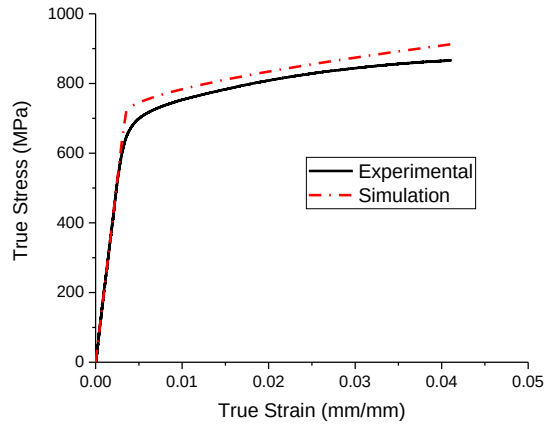

Fig. 4.57: Comparison of simulation and experimental true stress-true strain curves for 400°C at $0.0001s^{-1}$ strain rate.

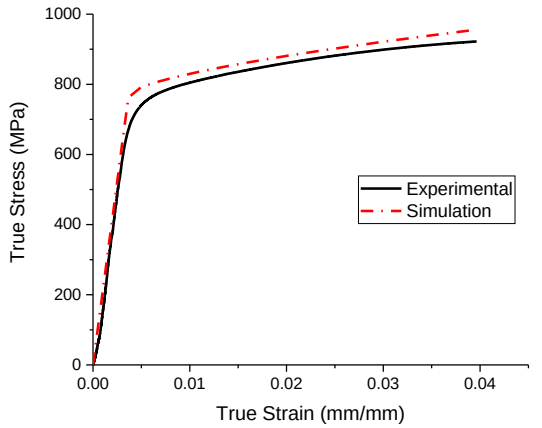

Fig. 4.58: Comparison of simulation and experimental true stress-true strain curves for 400°C at $0.001s^{-1}$strain rate.

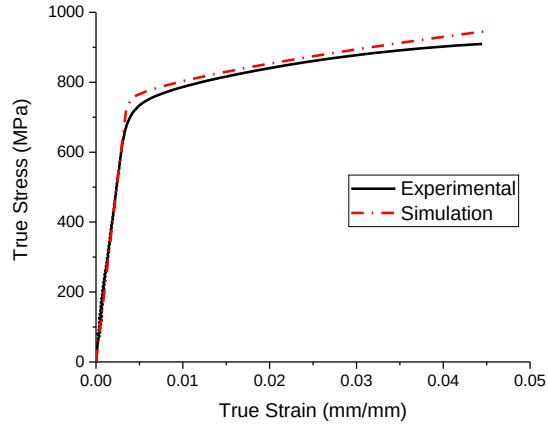

Fig. 4.59: Comparison of simulation and experimental true stress-true strain curves for 400°C at $0.01s^{-1}$ strain rate.

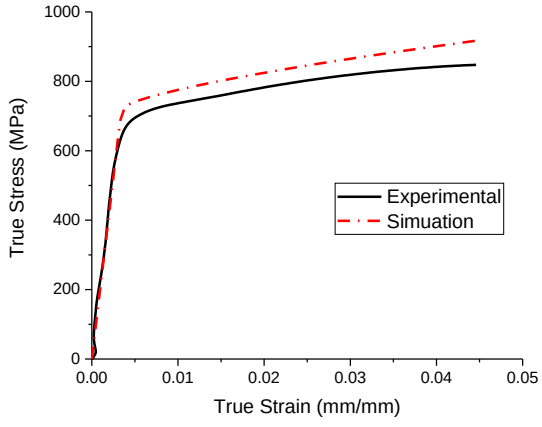

Fig. 4.60: Comparison of simulation and experimental true stress-true strain curves for 400°C at $0.1s^{-1}$ strain rate.

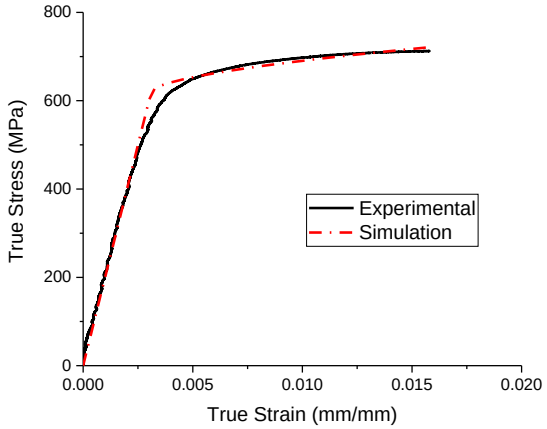

Fig. 4.61: Comparison of simulation and experimental true stress-true strain curves for 500°C at 0.0001s^{-1} strain rate.

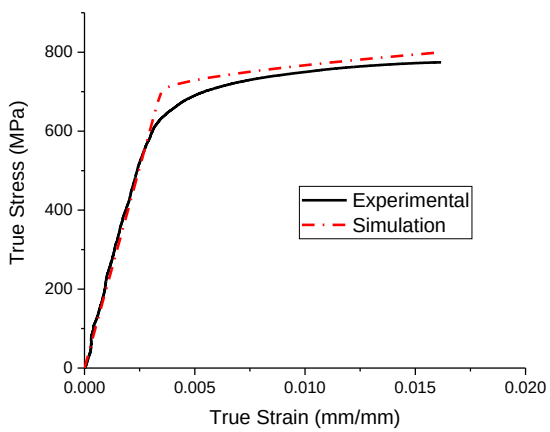

Fig. 4.62: Comparison of simulation and experimental true stress-true strain curves for 500°C at 0.001s^{-1}strain rate.

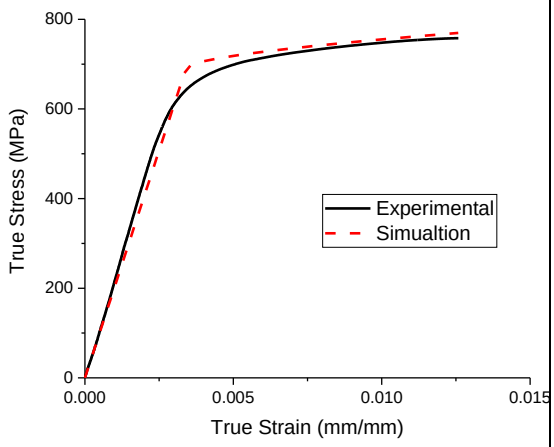

Fig. 4.63: Comparison of simulation and experimental true stress-true strain curves for 500°C at 0.01s^{-1} strain rate.

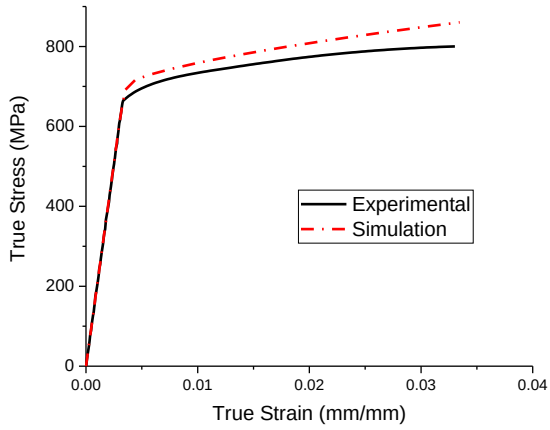

Fig. 4.64: Comparison of simulation and experimental true stress-true strain curves for 500°C at 0.1s^{-1} strain rate.

The prediction for the proposed model is validated using different strain rates and temperatures. For the proposed model, the material constants are captured in Table 3.5. Figs. 4.45 to 4.64 describes the flow curve proposed by the model for different strain rates and temperatures of the armour steel material. And we can clearly observe that the flow curve predicted by the proposed model tallies rationally well with the experiment curves which are depicted in Figs. 4.45 to 4.64, that describes the simulated flow behavior of strain rates variation from 0.0001s^{-1} to 0.1s^{-1} and the variation of temperature from 25°C to 500°C.

It is noticed that the low strain rate experiment shows high strain hardening behavior meanwhile high strain rate experiment results in very little strain hardening behavior. The increasing yield stress and consecutive decrease of strain hardening behavior (nature of flow curve) for strain rates and temperatures are perfectly addressed by the proposed model. However, it can be observed from Figs. 4.45 to 4.64 that both yield stress and strain hardening

behavior decrease with increase of temperature. And the value of yield stress is nearly constant for increase of yield strain rate but the strain hardening behavior decreases with increase of strain rate. Of course, these models are capable of predicting high temperature and strain rate behavior of armour steel material where both the yield stress and strain hardening behavior decreases with increase of temperature.

Therefore, it can be stated that the proposed model is capable of addressing yield stress and simultaneously the strain hardening behavior at numerous temperatures and strain rates more accurately. These Figs. 4.45 to 4.64 clearly demonstrates that the flow stress depicted by the proposed model can detect the experiment data over the entire range of strain, strain rate and temperature. The marginal deviation predicted for few temperatures can be basically attributed to the scatter in the experimental data.

For validation of the proposed constitutive model for armour material, simulation based on numerical approach is performed by dynamic tension tests. The specimen is meshed that has been depicted in Fig. 3.41 the specimen's dimensions are considered in one quarter of the test for reducing the computational time. The motive of the simulation is to compare between the true stress vs. true strain curves that is obtained from the experimental results with the results of numerical simulation.

The numerical simulation matches well with the experimental results of the proposed model constitutive relationship. In this work only the flow behaviour of the curves is inspected and modelled phenomenologically. The comparison appears at large deformation when necking arises. A simple answer for such differences can be that the geometrical instability is not admitted for the analytical form of the constitutive relation. Exactly similar type of observation was also proposed in case of mild steel ES by Rushinek et al. [37].

Chapter 5

5. Validation of the model:

5.1 Finite element modelling of notch specimens:

For verification, the constitutive model is calibrated and implemented, five different types of tensile tests on the specimen of armour material are simulated using the commercial FE code Abaqus and the simulated force–elongation curves are compared with the experimented data. By considering the low strain rates that are involved in the tests, the effect of inertia has been neglected. In this material model using Abaqus Standard, the modified J–C constitutive relation and modified J–C failure models are implemented as user defined model (UMAT sub-routine).

The values for the parameters of proposed material model are determined through tensile tests described in Section 3.1 and presented in Table 3.5 that are used. Using UMAT subroutine, a two-stage damage evolution rule has also been implemented. In the user defined material model (UMAT) sub-routine, the J-C damage parameters value of the armour steel material has been implemented and that data was been taken from existing literature of Arkadeb Banerjee et al [75].

The representative of FE meshing for a notched specimen and the meshes that are deformed of the notched flat specimens are depicted in Figs. 5.65 and 5.66. Considering the symmetry of the specimens and the loads for reduction of computational time, one – half of the model has been prepared for the notch flat specimens.

The specimens are modelled with one integration point with the use of 8-node hexahedral element (C3D8). At the free end, displacement is considered as input and from the support end, the reactions are measured to determine the load.

Three additional simulations of armour steel are being carried out for different dimensional flat specimens in 25°C temperature and at $0.0001s^{-1}$ strain rate and are compared with experimental load-displacement curves to prove the model (shown in Figs. 5.67 to 5.69).

For the five cases of tensile test, the FE simulated force–elongation curves are compared between the experimental observations in Figs. 5.70 to 5.74. Logically, good agreement is characterised with respect to the maximum load as well as the elongation related to fracture. Also, the damage law that is implemented in the programme is shown in Figs. 5.70 to 5.74.

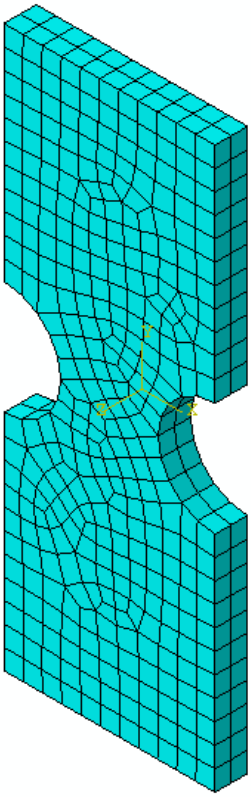

Fig. 5.65: Meshing of notch one-half tensile specimen

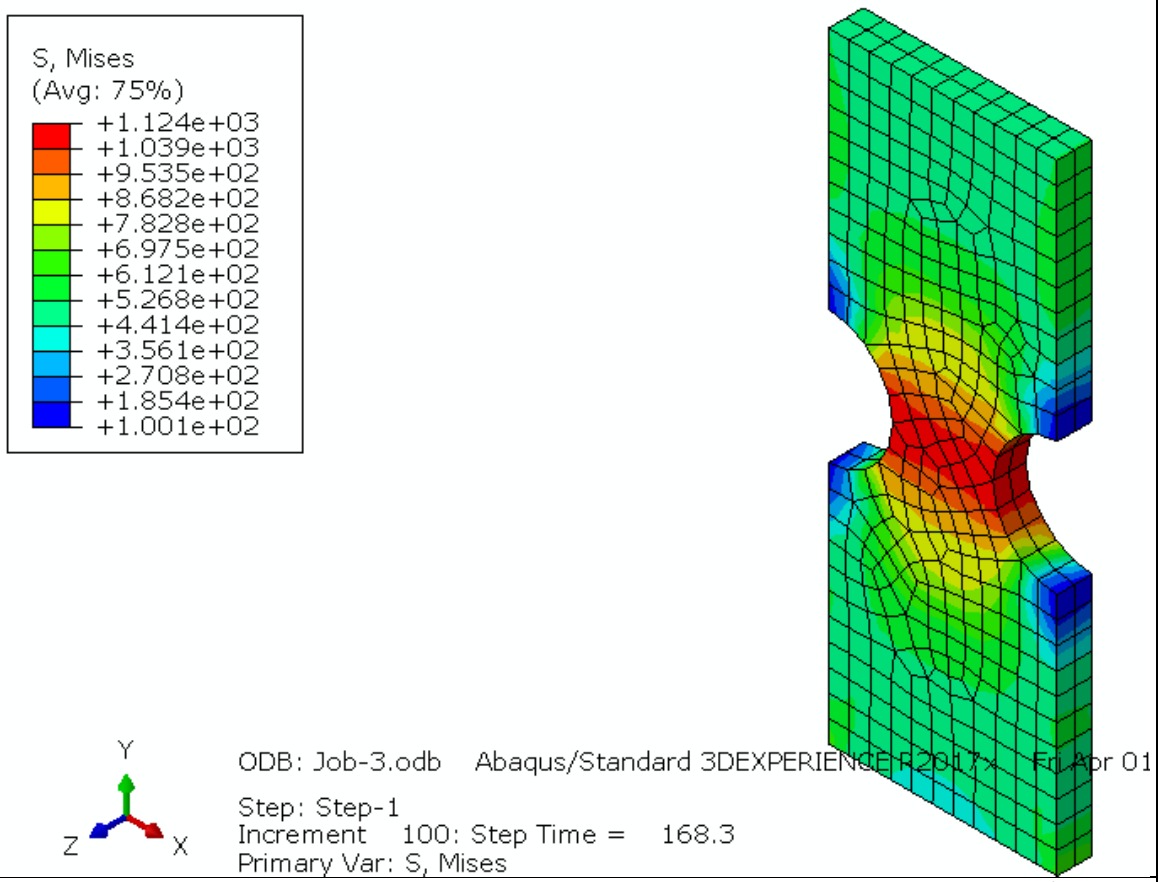

Fig. 5.66: Von-Mises stress distribution of notch specimen at 25°C and $0.0001s^{-1}$ strain rate.

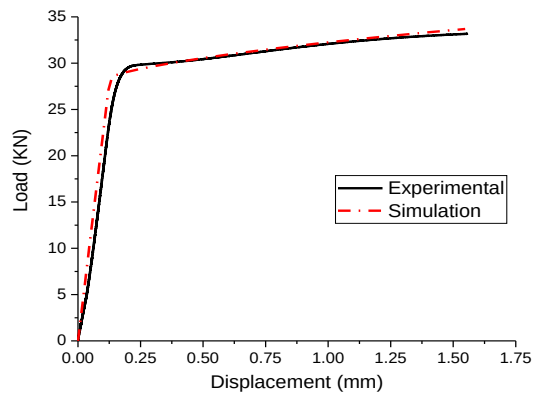

Fig. 5.67: Comparison of simulated and experimental load-displacement curve at 25°C temperature and $0.0001s^{-1}$ strain rate of flat specimen of 31.59 mm (gauge length)_5.94 mm (width)_5.96mm (thickness).

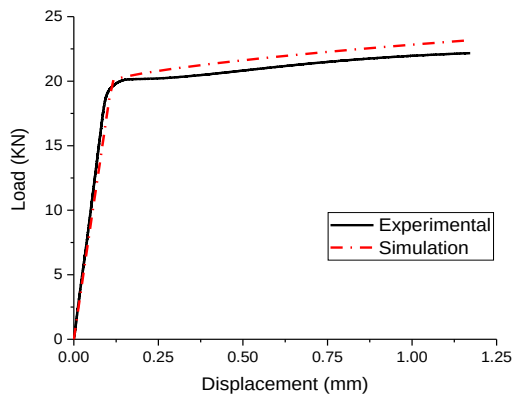

Fig. 5.68: Comparison of simulated and experimental load-displacement curve at 25°C temperature and $0.0001s^{-1}$ strain rate of flat specimen of 30.81 mm (gauge length)_5.96 mm (width)_3.93 mm (thickness).

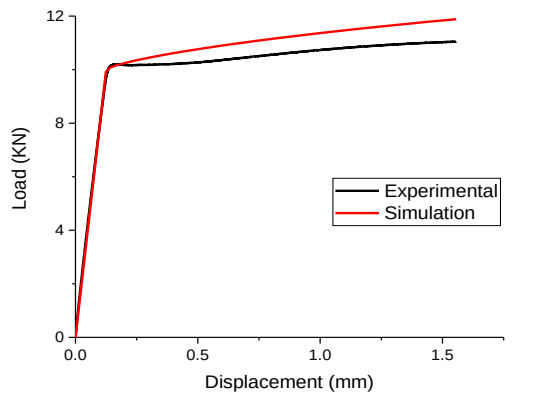

Fig. 5.69: Comparison of simulated and experimental load-displacement curve at 25°C temperature and $0.0001s^{-1}$ strain rate of flat specimen of 31.12 mm (gauge length)_5.93 mm (width)_1.99mm (thickness).

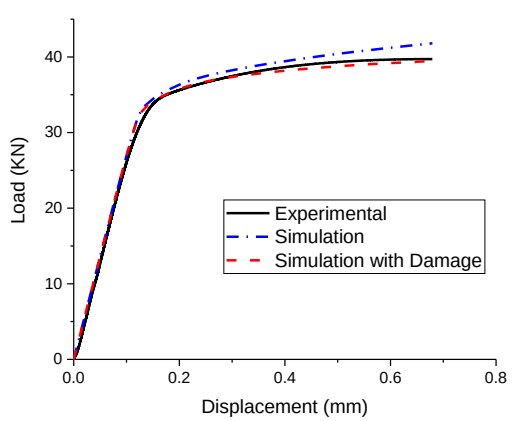

Fig. 5.70: Comparison of experimental, simulation and simulation with damage load vs. displacement curves for 25°C temperature and at $0.0001s^{-1}$ strain rate of round notch flat specimen at 32.21 mm (gauge length)_9.98 mm (width)_5.96mm (thickness)_3.90 mm (diameter).

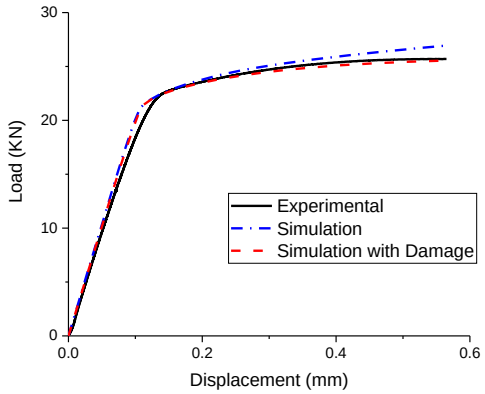

Fig. 5.71: Comparison of experimental, simulation and simulation with damage load vs. displacement curves for 25°C temperature and at $0.0001s^{-1}$ strain rate of round notch flat specimen at 31.58 mm (gauge length)_10.00 mm (width)_3.90 mm (thickness)_3.90 mm (diameter).

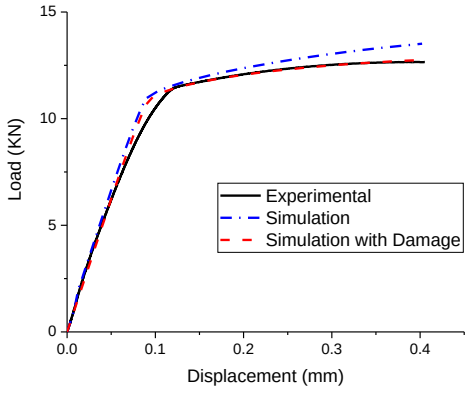

Fig. 5.72: Comparison of experimental, simulation and simulation with damage load vs. displacement curves for 25°C temperature and at $0.0001s^{-1}$ strain rate of round notch flat specimen at 29.59 mm (gauge length)_9.98 mm (width)_2.00 mm (thickness)_3.96 mm (diameter).

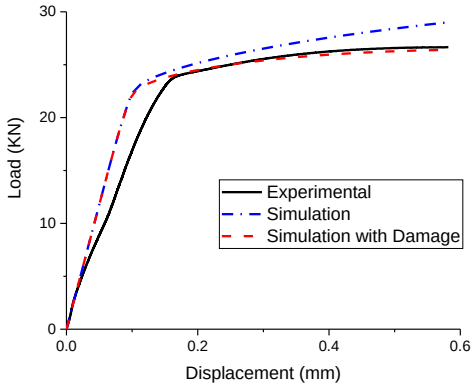

Fig. 5.73: Comparison of experimental, simulation and simulation with damage load vs. displacement curves for 25°C temperature and at $0.0001s^{-1}$ strain rate of round notch flat specimen at 34.57 mm (gauge length)_13.98 mm (width)_3.92mm (thickness)_8.00 mm (diameter).

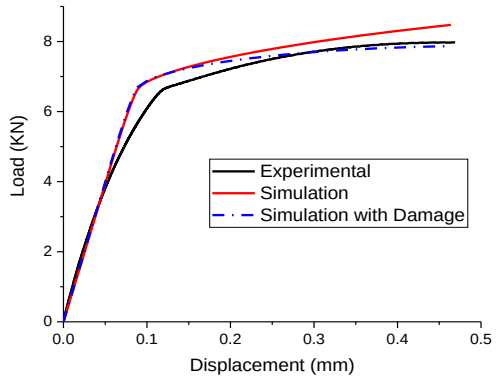

Fig. 5.74: Comparison of experimental, simulation and simulation with damage load vs. displacement curves for 25°C temperature and at $0.0001s^{-1}$ strain rate of round notch flat specimen at 34.92 mm (gauge length)_13.99 mm (width)_1.96 mm (thickness)_7.98 mm (diameter).

It is observed that the pattern of the experimented and simulated curves is similarly related and the time to reach the peak force value also satisfies. The drop in the force for both simulated and experimented plots occur at the particular time and displacement. The nature of the drop also has been modelled accurately. The successful prediction of the maximum load and the nature of its drop with time validates the damage distribution as well as the damage growth model used in the FE simulation. The simulated value is in the form of variation of the force that is applied on the specimen with respect to displacement is also found to be match appreciably with the experimental value. Thus, this model is found to satisfactorily represent the behaviour of the armour steel material in a low to moderately strain rates event and room to high temperatures.

Chapter 6

6. Summary, Conclusion and Future scope of the work

6.1 Summary of the present work:

To summarize the present material modelling, the work mainly focuses on the constitutive relationship of strain rate and temperature dependent behaviour of metals, especially in case of RHA steel. Moreover, Finite element analysis has been the first choice for simulating the response of armour steel plate in this work. A brief chapter-wise summarization has been depicted which is as follows:

Chapter 1: A brief introductory part of the work that provides us a good knowledge about the material used, its advantages, its application as well as the modelling aspect of the material. The chapter in its latter part also describes the development perspective of strain rate and temperature dependence of the material model. An overview of the literatures also has been presented that motivates the present work along with the objective that completes this chapter.

Chapter 2: This chapter begins with sub-parts consisting two important contents. The starting context enters into the in-depth details of the material i.e., Armour Steel. Its classification along with the physical material properties has been vastly described. The present work has been carried out with RHA steel, so its description, application, chemical composition, heat treatment method is its theoretical contents that ends with a microstructural image of the material. The ending part of this chapter is the experimental evaluation that attracts this work. It enters into the procedural steps of tensile test continuing with the results of the mechanical properties and exits with the flow properties of the tensile experiment.

Chapter 3: The main focus of this work is presented in this chapter that defines the modelling perspective as well the simulation aspect. It starts with the modelling of the tensile properties with the effects of temperature and strain rate. The analytical derivation of the constitutive equations with merging into a single set of equations and validation with the experimental curves resulted in developing a great concept of flow stress scenario.

Now comes the simulation part of this experiment. The emerging concept begins with the use of Finite Element Analysis (FEA) implementing it with the software named Abaqus. But due to unavailability of this material model sub-routine in the Abaqus commercial package library, we constructed our own subroutine using the option of user defined material model sub-routine or rather UMAT sub-routine.

Here, the simulation methodology is described in a vast format. Begins with the Pre-processing steps following the solution analysis of FEA continuing with the backward Euler integration scheme and ending with post processing techniques. And the completion of this chapter happens.

Chapter 4: Moving on, this chapter describes the result and discussion part of the proposed model. The experimental results of the uni-axial tensile test have been compared with the simulation resultant curves in the variational form of true stress verses true strain and a brief idea has been extracted from the curves that shows a great coordination between the two that has been stated as the discussion topic in this chapter.

Chapter 5: This chapter validates the experimental curves with the simulation results in following ways. The specimen of the proposed model is round and regular in nature where the True stress verses true strain curves are validated in Chapter 4. But in this section to prove that the model is not only applicable for round and regular specimen but also for different specimens like that of flat specimen of regular as well as complex geometry nature, we conducted uni-axial tensile test on the before mentioned specimens and constructed curves of load verses displacement. And validation has been done comparing the experimental results with simulation analysis as well as simulation containing damage properties.

6.2 Conclusion:

The effect of both the strain rate and temperature on tensile properties are investigated at different temperatures (25°C, 200 °C, 300°C, 400°C and 500°C) and strain rates (0.0001 s^{-1}, 0.001 s^{-1}, 0.01 s^{-1} and 0.1 s^{-1}). Tensile properties that are observed at the above-mentioned ranges of temperature and strain rate shows variation along with the scatter instead of any monotonic trend. Direct curve fitting methodology is not suitable to correlate the variations of the flow stress with temperature and strain rate. Average method is applied to identify the appropriate relationship for a constant temperature and strain rate. For the constitutive model, the material parameters are then obtained by using experimental tensile results at various ranges of strain rate and low temperature.

For verifying whether the obtained material parameters are independent of the specimen geometry, we carried out simulation using finite element analysis for the obtained tensile test results at reference temperature (25°C) and reference strain rate ($0.0001s^{-1}$) in a flat notch and also without notch specimens and lastly it was validated with the experimental results. Finally, the constants extracted from the model and the law of damage growth have been used successfully for analysing the flat notch specimen of the armour steel material. A good coordination is observed between the curve obtained from the finite element stress strain results and the curve obtained from the experimental stress strain results. The relationship between the obtained results of the experiment along with the material parameters is observed to be applicable in general aspect for elevated temperatures and for higher strain rate.

6.3 Future scope:

The present stress-based modelling is actually a narrow dimensional component level study which still has numerous investigating pathways to research as a future aspect. Some of research studies as future work that needs still a limelight is as follows:

1. The material modelling is basically developed from uniaxial tensile tests at low to moderate strain rates ($10^{-4}s^{-1}$ to $10^{-1}s^{-1}$) and room to elevated temperatures (25°C to 500°C). A similar material modelling can be developed for higher strain rates and at cryogenic temperature conditions.
2. For rolled homogeneous armour (RHA) steel material, by uniaxial tensile testing for wide ranges of elevated temperature and strain rate, the phenomenon of dynamic strain ageing is prevailing or not can be identified.
3. Basically, this modelling is performed for RHA material but in near future there is definitely a scope is prevailing for other materials also.

References:

[1] I.F.B. Tytler, N.H. Thompson, H. Norma, B.. Jones, P.J. Wormell, Vehicles and bridging, Brassey's Defence Publishers, 1985.

[2] R. Ogorkiewicz, Armored Fighting Vehicles (AFV), 2006.

[3] A. Rusineka, J.A. Rodríguez-Martínez, Thermo-viscoplastic constitutive relation for aluminium alloys, modeling of negative strain rate sensitivity and viscous drag effects, Mater. Des. 30 (2009) 4377–4390.

[4] G.R. Johnson, W.H. Cook, A Constitutive Model and Data for Metals Subjected to Large Strains, High Strain Rates, and High Temperature ., Proceeding's 7th Int. Symp. Ballist. (1983) 541–547.

[5] Zerilli Frank J., Armstrong Ronald W., Dislocation-mechanics-based constitutive relations for material dynamics calculations, J. Appl. Phys. 61 (1998) 1816. https://doi.org/10.1063/1.338024.

[6] H. Feng, M.N. Bassim, Finite element modeling of the formation of adiabatic shear bands in AISI 4340 steel, Mater. Sci. Eng. A. 266 (1999) 255–260.

[7] Lin Y. C., X.-M. Chen, A critical review of experimental results and constitutive descriptions for metals and alloys in hot working, Mater. Des. 32 (2011) 1733–1759. https://doi.org/10.1016/J.MATDES.2010.11.048.

[8] Z.T. Fu, W.Y. Yang, S.Q. Zeng, B.P. Guo, S.B. Hu, Identification of constitutive model parameters for nickel aluminum bronze in machining, Trans. Nonferrous Met. Soc. China. 26 (2016) 1105–1111. https://doi.org/10.1016/S1003-6326(16)64207-3.

[9] L. Chen, W. Sun, J. Lin, G. Zhao, G. Wang, Modelling of constitutive relationship, dynamic recrystallization and grain size of 40Cr steel during hot deformation process, Results Phys. 12 (2019) 784–792. https://doi.org/10.1016/J.RINP.2018.12.046.

[10] L. LIU, Y. xin WU, H. GONG, K. WANG, Modification of constitutive model and evolution of activation energy on 2219 aluminum alloy during warm deformation process, Trans. Nonferrous Met. Soc. China. 29 (2019) 448–459. https://doi.org/10.1016/S1003-6326(19)64954-X.

[11] S. Huang, A.S. Khan, Modeling the mechanical behaviour of 1100-0 aluminum at different strain rates by the bodner-partom model, Int. J. Plast. 8 (1992) 501–517. https://doi.org/10.1016/0749-6419(92)90028-B.

[12] Babak Farrokh, S.Khan Akhtar, Grain size, strain rate, and temperature dependence of flow stress in ultra-fine grained and nanocrystalline Cu and Al: Synthesis, experiment, and constitutive modeling, Int. J. Plast. 25 (2009) 715–732. https://doi.org/10.1016/J.IJPLAS.2008.08.001.

[13] Kotkunde Nitin, Deole Aditya D., Gupta Amit Kumar, Singh Swadesh Kumar, Comparative study of constitutive modeling for Ti–6Al–4V alloy at low strain rates and elevated temperatures, Mater. Des. 55 (2014) 999–1005. https://doi.org/10.1016/J.MATDES.2013.10.089.

[14] Rusinek A., Klepaczko J. R., Shear testing of a sheet steel at wide range of strain rates and a constitutive relation with strain-rate and temperature dependence of the flow stress, Int. J. Plast. 17 (2001) 87–115. https://doi.org/10.1016/S0749-6419(00)00020-6.

[15] Abed F. H., Voyiadjis G. Z., A consistent modified Zerilli-Armstrong flow stress model for BCC and FCC metals for elevated temperatures, Acta Mech. 2005 1751. 175 (2005) 1–18. https://doi.org/10.1007/S00707-004-0203-1.

[16] Bodner S. R., Partom Y., Constitutive Equations for Elastic-Viscoplastic Strain-Hardening Materials, J. Appl. Mech. 42 (1975) 385–389. https://doi.org/10.1115/1.3423586.

[17] Wu He, Xu Wenchen, Wang Si Bing, Yang Zhong Ze, Chen Yu, Teng Bugang, Shan Debin, Guo Bin, A cellular automaton coupled FEA model for hot deformation behavior of AZ61 magnesium alloys, J. Alloys Compd. 816 (2020) 152562. https://doi.org/10.1016/J.JALLCOM.2019.152562.

[18] Mecking H., Kocks U. F., Kinetics of flow and strain-hardening, Acta Metall. 29 (1981) 1865–1875. https://doi.org/10.1016/0001-6160(81)90112-7.

[19] Seong Yujin, Yim Dami, Jang Min Ji, Park Jeong Min, Park Seong Jin, Kim Hyoung Seop, Physics-Based Constitutive Model of Porous Materials for Die/Isostatic Compaction of Metallic Powders, Met. Mater. Int. 26 (2020) 221–229. https://doi.org/10.1007/S12540-019-00317-Z/FIGURES/9.

[20] Badrish Anand, Morchhale Ayush, Kotkunde Nitin, Singh Swadesh Kumar, Influence of material modeling on warm forming behavior of nickel based super alloy, Int. J. Mater. Form. 13 (2020) 445–465. https://doi.org/10.1007/S12289-020-01548-X/FIGURES/21.

[21] Qiang Zhao, Wen Chen, Jun Lin, Shuhai Huang, Xiangsheng Xia, Hot deformation behavior of 7A04 aluminum alloy at elevated temperature: constitutive modeling and verification, Int. J. Mater. Form. 13 (2020) 293–302. https://doi.org/10.1007/S12289-019-01486-3/FIGURES/18.

[22] Saxena Ambuj, Kumaraswamy A., Kotkunde Nitin, Suresh Kurra, Constitutive Modeling of High-Temperature Flow Stress of Armor Steel in Ballistic Applications: A Comparative Study, J. Mater. Eng. Perform. 28 (2019) 6505–6513. https://doi.org/10.1007/S11665-019-04337-Z/TABLES/6.

[23] Su Nan, Chen Minghe, Zhang Wenliang, Xie Lansheng, Tang Weipeng, Constitutive Modeling of 17-4PH Stainless Steel Sheet at Elevated Temperature and Statistical Optimization, J. Mater. Eng. Perform. 29 (2020) 1194–1205. https://doi.org/10.1007/S11665-020-04648-6/FIGURES/12.

[24] Rudra Amitava, Ashiq Mohammad, Das Satyabrata, Dasgupta Rupa, Constitutive Modeling for Predicting High-Temperature Flow Behavior in Aluminum 5083+10 Wt Pct SiC p Composite, Metall. Mater. Trans. B Process Metall. Mater. Process. Sci. 50 (2019) 1060–1076. https://doi.org/10.1007/S11663-019-01531-1/FIGURES/21.

[25] TAO Zhi jun, FAN Xiao guang, YANG He, MA Jun, LI Heng, A modified Johnson–Cook model for NC warm bending of large diameter thin-walled Ti–6Al–4V tube in wide ranges of strain rates and temperatures, Trans. Nonferrous Met. Soc. China. 28 (2018) 298–308. https://doi.org/10.1016/S1003-6326(18)64663-1.

[26] Geng Peihao, Qin Guoliang, Zhou Jun, Zou Zengda, Hot deformation behavior and constitutive model of GH4169 superalloy for linear friction welding process, J. Manuf. Process. 32 (2018) 469–481. https://doi.org/10.1016/J.JMAPRO.2018.03.017.

[27] Zhang Hongming, Chen Gang, Chen Qiang, Han Fei, Zhao Zude, A physically-based constitutive modelling of a high strength aluminum alloy at hot working conditions, J. Alloys Compd. 743 (2018) 283–293. https://doi.org/10.1016/J.JALLCOM.2018.02.039.

[28] Bodunrin Michael Oluwatosin, Flow stress prediction using hyperbolic-sine Arrhenius constants optimised by simple generalised reduced gradient refinement, J. Mater. Res. Technol. 9 (2020) 2376–2386. https://doi.org/10.1016/J.JMRT.2019.12.070.

[29] Gupta Amit Kumar, Anirudh V. K., Singh Swadesh Kumar, Constitutive models to predict flow stress in Austenitic Stainless Steel 316 at elevated temperatures, Mater. Des. 43 (2013) 410–418. https://doi.org/10.1016/J.MATDES.2012.07.008.

[30] Wang Z. L., Shi H., Wang J. G., Mechanical Behavior and Damage Constitutive Model of Granite Under Coupling of Temperature and Dynamic Loading, Rock Mech. Rock Eng. 51 (2018) 3045–3059. https://doi.org/10.1007/S00603-018-1523-0/FIGURES/19.

[31] J. Shen, L. Hu, Y. Sun, Z. Wan, X. Feng, Y. Ning, A Comparative Study on Artificial Neural Network, Phenomenological-Based Constitutive and Modified Fields–Backofen Models to Predict Flow Stress in Ti-4Al-3V-2Mo-2Fe Alloy, J. Mater. Eng. Perform. 28 (2019) 4302–4315. https://doi.org/10.1007/S11665-019-04174-0/FIGURES/12.

[32] Lin Y. C., Dong Wen Yong, Zhou Mi, Wen Dong Xu, Chen Dong Dong, A unified constitutive model based on dislocation density for an Al-Zn-Mg-Cu alloy at time-variant hot deformation conditions, Mater. Sci. Eng. A. 718 (2018) 165–172. https://doi.org/10.1016/J.MSEA.2018.01.109.

[33] Rasaee Sajad, Mirzaei A. H., Almasi D., Constitutive modelling of Al7075 using the Johnson–Cook model, Bull. Mater. Sci. 43 (2020) 1–8. https://doi.org/10.1007/S12034-019-1987-X/FIGURES/12.

[34] Zhao Han, Gary Gérard, The testing and behaviour modelling of sheet metals at strain rates from 10−4 to 104 s−1, Mater. Sci. Eng. A. 207 (1996) 46–50. https://doi.org/10.1016/0921-5093(95)10017-2.

[35] Zhao Han, Gary Gérard, On the use of SHPB techniques to determine the dynamic behavior of materials in the range of small strains, Int. J. Solids Struct. 33 (1996) 3363–3375. https://doi.org/10.1016/0020-7683(95)00186-7.

[36] N. Peixinho, N. Jones, A. Pinho, Experimental and numerical study in axial crushing of thin walled sections made of high-strength steels, J. Phys. IV. 110 (2003) 717–722. https://doi.org/10.1051/JP4:20020778.

[37] A. Rusinek, R. Zaera, J.R. Klepaczko, Constitutive relations in 3-D for a wide range of strain rates and temperatures – Application to mild steels, Int. J. Solids Struct. 44 (2007) 5611–5634. https://doi.org/10.1016/J.IJSOLSTR.2007.01.015.

[38] J. Klepaczko, J. Duffy, Strain Rate History Effects in Body-Centered-Cubic Metals, Am. Soc. Test. Mater. (1982) 251–268.

[39] Follansbee P. S., Kocks U. F., A constitutive description of the deformation of copper based on the use of the mechanical threshold stress as an internal state variable, Acta Metall. 36 (1988) 81–93. https://doi.org/10.1016/0001-6160(88)90030-2.

[40] Tong Wei, Clifton Rodney J., Huang Shihui, Pressure-shear impact investigation of strain rate history effects in oxygen-free high-conductivity copper, J. Mech. Phys. Solids. 40 (1992) 1251–1294. https://doi.org/10.1016/0022-5096(92)90015-T.

[41] Bodner S. R., Rubin M. B., Modeling of hardening at very high strain rates, J. Appl. Phys. 76 (1998) 2742. https://doi.org/10.1063/1.357578.

[42] Frutschy K. J., Clifton R. J., High-temperature pressure-shear plate impact experiments on ofhc copper, J. Mech. Phys. Solids. 46 (1998) 1723–1744. https://doi.org/10.1016/S0022-5096(98)00055-6.

[43] Frutschy K. J., Clifton R. J., High-temperature pressure-shear plate impact experiments using pure tungsten carbide impactors, Exp. Mech. 1998 382. 38 (1998) 116–125. https://doi.org/10.1007/BF02321654.

[44] E. Nes, Modelling of work hardening and stress saturation in FCC metals, Prog. Mater. Sci. 41 (1997) 129–193. https://doi.org/10.1016/S0079-6425(97)00032-7.

[45] E. Van der Giessen, A. Needleman, Discrete dislocation plasticity: a simple planar model, Model. Simul. Mater. Sci. Eng. 3 (1995) 689. https://doi.org/10.1088/0965-0393/3/5/008.

[46] M. Ortiz, E.A. Repetto, H. Si, A continuum model of kinetic roughening and coarsening in thin films, J. Mech. Phys. Solids. 47 (1999) 697–730. https://doi.org/10.1016/S0022-5096(98)00102-1.

[47] W.M. Ashmawi, M.A. Zikry, Grain boundary effects and void porosity evolution, Mech. Mater. 35 (2003) 537–552. https://doi.org/10.1016/S0167-6636(02)00269-7.

[48] Molinari A., Ravichandran G., Constitutive modeling of high-strain-rate deformation in metals based on the evolution of an effective microstructural length, Mech. Mater. 37 (2005) 737–752. https://doi.org/10.1016/J.MECHMAT.2004.07.005.

[49] S. Nemat-Nasser, Y.F. Li, J.B. Isaacs, Experimental/ computational evaluation of flow stress at high strain rates with application to adiabatic shear banding, Mech. Mater. 17 (1994) 111–134. https://doi.org/10.1016/0167-6636(94)90053-1.

[50] S. Nemat-Nasser, J.B. Isaacs, Direct measurement of isothermal flow stress of metals at elevated temperatures and high strain rates with application to Ta and TaW alloys, Acta Mater. 45 (1997) 907–919. https://doi.org/10.1016/S1359-6454(96)00243-1.

[51] L. Riqiang, S.K. Akhtar, A critical review of experimental results and constitutive models for BCC and FCC metals over a wide range of strain rates and temperatures, Int. J. Plast. 15 (1999) 963–980. https://doi.org/10.1016/S0749-6419(99)00021-2.

[52] J.A. Rodríguez-Martínez, M. Rodríguez-Millán, A. Rusinek, A. Arias, A dislocation-based constitutive description for modeling the behavior of FCC metals within wide ranges of strain rate and temperature, Mech. Mater. 43 (2011) 901–912. https://doi.org/10.1016/J.MECHMAT.2011.09.008.

[53] J. Richeton, S. Ahzi, K.S. Vecchio, F.C. Jiang, R.R. Adharapurapu, Influence of temperature and strain rate on the mechanical behavior of three amorphous polymers: Characterization and modeling of the compressive yield stress, Int. J. Solids Struct. 43 (2006) 2318–2335. https://doi.org/10.1016/J.IJSOLSTR.2005.06.040.

[54] S. Nemat-Nasser, W.G. Guo, D.P. Kihl, Thermomechanical response of AL-6XN stainless steel over a wide range of strain rates and temperatures, J. Mech. Phys. Solids. 49 (2001) 1823–1846. https://doi.org/10.1016/S0022-5096(00)00069-7.

[55] M. Ruiz De Sotto, P. Longère, V. Doquet, J. Papasidero, A constitutive model for a rate and temperature-dependent, plastically anisotropic titanium alloy, Int. J. Plast. 134 (2020) 102777. https://doi.org/10.1016/J.IJPLAS.2020.102777.

[56] A. Banerjee, S. Dhar, S. Acharyya, D. Datta, N. Nayak, Determination of Johnson cook material and failure model constants and numerical modelling of Charpy impact test of armour steel, Mater. Sci. Eng. A. 640 (2015) 200–209. https://doi.org/10.1016/J.MSEA.2015.05.073.

[57] A. Uenishi, C. Teodosiu, Constitutive modelling of the high strain rate behaviour of interstitial-free steel, Int. J. Plast. 20 (2004) 915–936. https://doi.org/10.1016/J.IJPLAS.2003.06.004.

[58] D. Samantaray, S. Mandal, U. Borah, A.K. Bhaduri, P. V. Sivaprasad, A thermo-viscoplastic constitutive model to predict elevated-temperature flow behaviour in a titanium-modified austenitic stainless steel, Mater. Sci. Eng. A. 526 (2009) 1–6. https://doi.org/10.1016/J.MSEA.2009.08.009.

[59] H. Yu, Y. Guo, X. Lai, Rate-dependent behavior and constitutive model of DP600 steel at strain rate from 10−4 to 103 s−1, Mater. Des. 30 (2009) 2501–2505. https://doi.org/10.1016/J.MATDES.2008.10.001.

[60] K. Wang, S. Ahzi, R. Matadi Boumbimba, N. Bahlouli, F. Addiego, Y. Rémond, Micromechanical modeling of the elastic behavior of polypropylene based organoclay nanocomposites under a wide range of temperatures and strain rates/frequencies, Mech. Mater. 64 (2013) 56–68. https://doi.org/10.1016/J.MECHMAT.2013.04.009.

[61] S.K. Paul, Predicting the flow behavior of metals under different strain rate and temperature through phenomenological modeling, Comput. Mater. Sci. 65 (2012) 91–99. https://doi.org/10.1016/J.COMMATSCI.2012.06.039.

[62] S.K. Paul, A. Raj, P. Biswas, G. Manikandan, R.K. Verma, Tensile flow behavior of ultra low carbon, low carbon and micro alloyed steel sheets for auto application under low to intermediate strain rate, Mater. Des. 57 (2014) 211–217. https://doi.org/10.1016/J.MATDES.2013.12.047.

[63] W.S. Lee, C.Y. Liu, The effects of temperature and strain rate on the dynamic flow behaviour of different steels, Mater. Sci. Eng. A. 426 (2006) 101–113. https://doi.org/10.1016/J.MSEA.2006.03.087.

[64] S. Paul, P. Dey, S. Bhattacharjee, S.K. Acharyya, P. Sahoo, J. Chattopadhyay, Phenomenological modelling of flow behaviour of 20MnMoNi55 reactor pressure vessel steel at cryogenic temperature with different strain rates, Def. Technol. 15 (2019) 326–337. https://doi.org/10.1016/J.DT.2018.08.007.

[65] Hecker S. S., Stout M. G., Staudhammer K. P., Smith J. L., Effects of Strain State and Strain Rate on Deformation-Induced Transformation in 304 Stainless Steel: Part I. Magnetic Measurements and Mechanical Behavior, Metall. Trans. A 1982 134. 13 (1982) 619–626. https://doi.org/10.1007/BF02644427.

[66] M.Z. Shah Khan, S.J. Alkemade, G.M. Weston, Fracture Studies on High Hardness BISALLOY 500(R) Steel. | National Technical Reports Library - NTIS, 1998. https://ntrl.ntis.gov/NTRL/dashboard/searchResults/titleDetail/ADA348496.xhtml (accessed May 16, 2022).

[67] S.J. Manganello, K.H. Abbot, Metallurgical factors affecting the ballistic behavior of steel targets, J. Mater. JMLSA. 7 (1972) 231–239.

[68] G.E. Dieter, Mechanical metallurgy, 1981.

[69] P.W. Leach, R.L. Woodward, The influence of microstructural anisotropy on the mode of plate failure during projectile impact, J. Mater. Sci. 1985 203. 20 (1985) 854–858. https://doi.org/10.1007/BF00585726.

[70] R.L. Woodward, N.J. Baldwin, Oblique Perforation of Targets by Small Armour-Piercing Projectiles, J. Mech. Eng. Sci. 21 (1979) 85–91.

[71] C. Zener, J.H. Hollomon, Effect of Strain Rate Upon Plastic Flow of Steel, J. Appl. Phys. 15 (2004) 22. https://doi.org/10.1063/1.1707363.

[72] R.F. Recht, Catastrophic Thermoplastic Shear, J. Appl. Mech. 31 (1964) 189–193. https://doi.org/10.1115/1.3629585.

[73] T.B. Bhat, Science of armour materials, Def. Sci. J. 35 (1985) 219–223.

[74] M.R. Lin, R.H. Wagoner, An experimental investigation of deformationinduced heating during tensile testing, Metall. Mater. Trans. A 1991 186. 18 (1987) 1035–1042. https://doi.org/10.1007/BF02668552.

[75] A. Banerjee, S. Dhar, S. Acharyya, D. Datta, N. Nayak, An Experimental Determination of Johnson Cook Material and Failure Model Constants for Armour Steel, Appl. Mech. Mater.592–594 (2014) 990–995. https://doi.org/10.4028/WWW.SCIENTIFIC.NET/AMM.592-594.990.